Historical Evaluation and Future Prediction of Eastern North American and Western Atlantic Extratropical Cyclones in the CMIP5 Models during the Cool Season

BRIAN A. COLLE, ZHENHAI ZHANG, KELLY A. LOMBARDO, EDMUND CHANG, PING LIU, AND MINGHUA ZHANG

School of Marine and Atmospheric Sciences, Stony Brook University, Stony Brook, New York

(Manuscript received 26 July 2012, in final form 14 March 2013)

ABSTRACT

Extratropical cyclone track density, genesis frequency, deepening rate, and maximum intensity distributions over eastern North America and the western North Atlantic were analyzed for 15 models from phase 5 of the Coupled Model Intercomparison Project (CMIP5) for the historical period (1979–2004) and three future periods (2009–38, 2039–68, and 2069–98). The cyclones were identified using an automated tracking algorithm applied to sea level pressure every 6 h. The CMIP5 results for the historical period were evaluated using the Climate Forecast System Reanalysis (CFSR). The CMIP5 models were ranked given their track density, intensity, and overall performance for the historical period. It was found that six of the top seven CMIP5 models with the highest spatial resolution were ranked the best overall. These models had less underprediction of cyclone track density, more realistic distribution of intense cyclones along the U.S. East Coast, and more realistic cyclogenesis and deepening rates. The best seven models were used to determine projected future changes in cyclones, which included a 10%–30% decrease in cyclone track density and weakening of cyclones over the western Atlantic storm track, while in contrast there is a 10%–20% increase in cyclone track density over the eastern United States, including 10%–40% more intense (<980 hPa) cyclones and 20%–40% more rapid deepening rates just inland of the U.S. East Coast. Some of the reasons for these CMIP5 model differences were explored for the selected models based on model generated Eady growth rate, upper-level jet, surface baroclinicity, and precipitation.

1. Introduction

a. Background

During the last decade there has been growing interest in assessing whether climatic extremes are changing as a result of global warming. Along the eastern United States this research is important since there is a relatively large population that is vulnerable to extreme temperature, precipitation, wind, and coastal flooding. During the cool season much of the high-impact weather over the Northeast United States is related to intense cyclones that often track near the coast. Associated with these storms are heavy snow (Novak et al. 2008), inland flooding (Colle 2003), and storm surge (Colle et al. 2008). Therefore, any change in the frequency and intensity of these midlatitude cyclones over the Northeast United States is of great interest given the potential catastrophic consequences. For example, coastal areas of the Northeast United States are extremely vulnerable to storm surge, with the problem likely to become worse as the sea level rises during the next 100 years (Colle et al. 2010).

During the past 50 years there has been a large interdecadal variability in midlatitude cyclones and their associated storm surge for the New York City (NYC) area (Zhang et al. 2000; Colle et al. 2010). For example, after a relatively active period in the early–mid-1990s for storm surge (4–5 flooding events around NYC), there were no significant NYC coastal flooding events from 1997 to 2009 (Colle et al. 2010). Hirsch et al. (2001) completed a ~50-yr climatology of East Coast winter storms (nor'easters) using the National Centers for Environmental Prediction (NCEP) global reanalysis and found interannual variations associated with ENSO (El Niño favors more nor'easters) as well as relatively large interdecadal variations. Future planning for the protection

Corresponding author address: Dr. Brian A. Colle, School of Marine and Atmospheric Sciences, Stony Brook University/SUNY, Stony Brook, NY 11794-5000.
E-mail: brian.colle@stonybrook.edu

DOI: 10.1175/JCLI-D-12-00498.1

of life and property in this populated Northeast region will require more knowledge of how the intensity, frequency, and track of midlatitude cyclones will change during the next several decades.

b. Past studies

Storm-track activity and extratropical cyclone changes have been diagnosed with phase 3 of the Coupled Model Intercomparison Project (CMIP3; Meehl et al. 2007). This report and Pinto et al. (2007) highlight an increase in storm-track activity in the middle–upper troposphere, which has been linked to an increase in the zonal-mean eddy kinetic energy that shifts poleward and to a slightly higher level (Yin 2005). This is consistent with an increasing temperature gradient at upper levels (250–500 hPa) related to cooling the lower stratosphere at higher latitudes and greater warming in the tropics related to increased vertical vapor flux and latent heat release.

Any increase in surface storm-track activity for the later twenty-first century has been limited to specific regions (Ulbrich et al. 2008), while the total number of surface cyclones in climate models has been shown to decrease for future periods (Lambert and Fyfe 2006; Geng and Sugi 2003; Bengtsson et al. 2006). Other studies also suggest a decrease in storms given a reduction in the north–south temperature gradients at low levels (Zhang and Wang 1997; Knippertz et al. 2000). Other analyses by Mickley et al. (2004) and Leibensperger et al. (2008) point to the reduced frequency of summer extratropical cyclones as well as displacements of tracks toward the north. Since there is larger warming in the lower troposphere at high latitudes from decreased albedo from less snow and ice cover, the meridional temperature gradient decreases near the surface and there is less potential for surface cyclogenesis. Even though there are competing upper- and lower-level changes to storm-track frequency, Held and O'Brien (1992) and Lunkeit et al. (1998) showed that baroclinic wave activity is more sensitive to lower-level changes rather than changes in the upper troposphere.

There is more uncertainty in how the frequency of more intense extratropical cyclones will change in the future. In several CMIP3 models there was an increase in more extreme cyclones (central pressure < 970 hPa) in the future experiments (Lambert and Fyfe 2006); however, the increase in intense cyclones is limited to some areas, depending on models and experiments. Regions near the British Isles and Aleutian Islands show an increase in some models (Geng and Sugi 2003; Pinto et al. 2007). This has been attributed to the latent heat release within these midlatitude storms (Carnell and Senior 1998). Latent heating may become more important for the intensity of these storms, since the globally averaged mean water vapor is projected to increase (Meehl et al. 2007).

Model spatial resolution is also important for the cyclone predictions. Jung et al. (2006) showed that a global model with T95 resolution can only simulate ~60% of the observed number of cyclones. Joyce et al. (2009) used a regional climate model over the western Atlantic to show a meridional shift of the local storm track along the U.S. East Coast is related to changes in the Gulf Stream SST gradient. Woollings et al. (2010) showed that the storm track over the western Atlantic is sensitive to how the Gulf Stream SST gradient is resolved in the model. A coarse-resolution SST (100–200-km grid spacing) yields more storms closer to the U.S. coast than a high-resolution (50–100 km) SST.

c. Motivation

More than 20 modeling groups completed simulations for phase 5 of the Coupled Model Intercomparison Project (CMIP5; Taylor et al. 2012), which provides a unique multimodel framework for assessing future climate change and the mechanisms responsible for model differences. The CMIP5 data are available at 6-h intervals, which for the first time allows for the tracking of cyclones in a multimodel framework. There is a historical period from the mid-nineteenth century to 2005 forced by observed atmospheric composition changes (reflecting both anthropogenic and natural sources) and time-evolving land cover. Each of the models is also run for different emission scenarios or representative concentration pathways (RCPs) for the future to 2100 or later. The future CMIP5 runs for this paper focus on the high-emission RCP8.5 scenario, since it was too computationally expensive to look at all scenarios. The CMIP5 models have been analyzed around North America for several different phenomena, such as temperature, precipitation, storm tracks, droughts, floods, and so on for both the historical (Sheffield et al. 2013) and the future period (Maloney et al. 2012, manuscript submitted to *J. Climate*). For example, Harvey et al. (2012) investigated the storm-track changes for the RCP4.5 scenario in the CMIP5 models and found that around 40% of the models in regions of the Northern Hemisphere had a future response that exceeded half the present-day interannual variability.

There have been several studies looking at the hemispheric changes in cyclone frequency and intensity, but more studies are needed to focus on particular regions or ocean basins in order to determine how well global models can predict the historical cyclone distributions before attempting to dynamically downscale these models. This paper will focus on the North Atlantic storm-track

entrance region from eastern North America to the central Atlantic region, which is of interest given the high population density along the U.S. East Coast.

Most studies use all available models in an ensemble with equal weighting in the assessment of future changes, but there are likely major differences between the models attributed to spatial resolution and physics. We evaluate the models separately, rank them, and use the selected members based on model performance during the historical period to determine if this approach has an impact on the future cyclone results. Finally, some physical reasons for the model difference in cyclone frequency and intensity have been explored in the western Atlantic storm-track region.

In summary, this paper will address the following questions:

- How well can the CMIP5 models simulate western Atlantic extratropical cyclones (density, intensity, genesis, and deepening) for the cool season (November–March) during the 1979–2004 historical period?
- How do the western Atlantic results compare with a regional U.S. East Coast domain?
- What is the impact of resolution on model performance and the utilization of the best subset of CMIP ensemble members based on past performance?
- Are there differences between models that may explain the cyclone differences, such as low-level temperature gradients and the upper-level jet?
- Is there any indication of future cyclone change in terms of frequency, intensity, or spatial distribution?

2. Data and methods

The Climate Forecast System Reanalysis (CFSR; Saha et al. 2010) at ~38-km grid spacing (64 vertical levels) was used to verify and compare the cyclone properties with the CMIP5 models for a few domains [East Coast land (ECL), East Coast water (ECW), and East Coast western and central Atlantic (EC-WA)] over eastern North America and the western North Atlantic (Fig. 1). The European Centre for Medium-Range Weather Forecasts (ECMWF) Interim Re-Analysis (ERA-Interim; Dee et al. 2011) was also used to test a 10-yr period (~58-km grid spacing and 60 levels), and the cyclone density results over the Atlantic were within 5% of the CFSR in most locations (not shown). This is consistent with Hodges et al. (2011), who showed that tracking cyclones in these and other reanalyses yielded similar results. The cyclone tracks were constructed using 6-hourly sea level pressure from the CFSR and 15 CMIP5 models (see Table 1 for all models and model expansions). If a CMIP5 model had more than one member available, only the first one was used, which included none of the physics or different initial start date perturbations. The surface cyclone tracking scheme used here is the one developed by Hodges (1994, 1995). Only the mean sea level pressure (MSLP) was used to do the tracking, which differs from other cyclone studies that used 850-hPa vorticity to track cyclones using the Hodges approach (Hoskins and Hodges 2002; Anderson et al. 2003). However, as will be shown later, we found that MSLP tracking worked at least as well as the vorticity tracking in our region of interest, which is eastern North America and the western Atlantic region shown in Fig. 1.

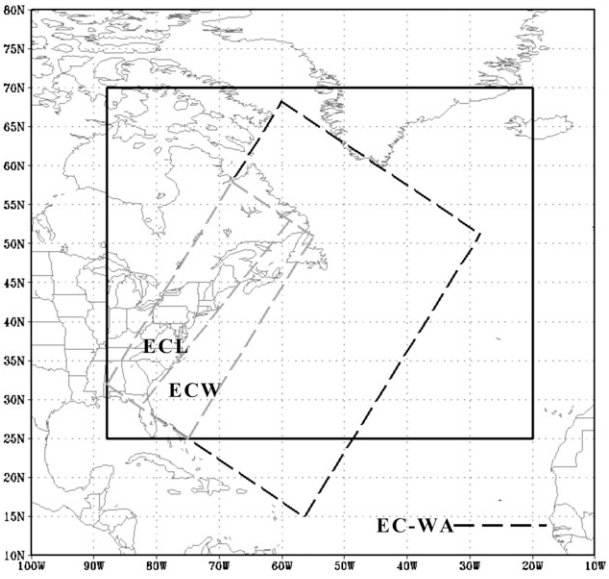

FIG. 1. The domains used in this study. The solid black box is the region used for the cyclone track density analysis, while the dashed box (EC-WA) is used for the cyclone intensity analysis over the western Atlantic, and the inner dashed ECL and ECW boxes areas are for the East Coast land and water analysis, respectively.

MSLP is strongly influenced by large spatial scales and strong background flows, so a spectral bandpass filter was used to preprocess the data. For example, a weak and fast moving cyclone can be masked by the background flow until it significantly developed. The planetary scales (i.e., total wavenumber equal or less than 5) are removed. Anderson et al. (2003) showed little sensitivity using wavenumber 5 or 7 for this filter. The data are also truncated at small scales (i.e., total wavenumber larger than 70). This is slightly larger than the wavenumber 63 cutoff used in Hodges et al. (2011) so that some smaller-scale cyclones can be identified.

The Hodges MSLP cyclone tracking involves four steps: segmentation, feature point detection, tracking, and filtering. Segmentation identifies the objects in the MSLP fields, which are the regions around minima in the MSLP field. The feature detection identifies suitable

TABLE 1. CMIP5 models evaluated and their attributes and full expansions. The seven relatively high-resolution models are in boldface.

Model	Center	Atmospheric horizontal resolution (lon × lat)	No. of model levels	Reference
Community Climate System Model, version 4 (CCSM4)	**National Center for Atmospheric Research**	**1.25° × 0.94°**	**26**	**Gent et al. (2011)**
EC-Earth Consortium (EC-Earth)	**EC-Earth Consortium**	**1.125° × 1.12°**	**62**	**Hazeleger et al. (2010)**
Meteorological Research Institute Coupled Atmosphere–Ocean General Circulation Model, version 3 (MRI-CGCM3)	**Meteorological Research Institute, Japan**	**1.125° × 1.12°**	**48**	**Yukimoto et al. (2012)**
Centre National de Recherches Météorologiques Coupled Global Climate Model, version 5.1 (CNRM-CM5.1)	**National Centre for Meteorological Research, France**	**1.4° × 1.4°**	**31**	**Michou et al. (2011)**
Model for Interdisciplinary Research on Climate, version 5 (MIROC5)	**Atmosphere and Ocean Research Institute (The University of Tokyo), National Institute for Environmental Studies, and Japan Agency for Marine-Earth Science and Technology, Japan**	**1.4° × 1.4°**	**40**	**Watanabe et al. (2011)**
Hadley Centre Global Environmental Model, version 2 - Earth System (HADGEM2-ES)	**Met Office Hadley Centre, United Kingdom**	**1.875° × 1.25°**	**38**	**Jones et al. (2011)**
Hadley Centre Global Environmental Model, version 2 - Carbon Cycle (HADGEM2-CC)	**Met Office Hadley Centre, United Kingdom**	**1.875° × 1.25°**	**60**	**Jones et al. (2011)**
Institute of Numerical Mathematics Coupled Model, version 4.0 (INM-CM4.0)	Institute of Numerical Mathematics, Russia	2.0° × 1.5°	21	Volodin et al. (2010)
L'Institut Pierre-Simon Laplace Coupled Model, version 5, coupled with NEMO, mid resolution (IPSL-CM5A-MR)	Institut Pierre Simon Laplace, France	2.50° × 1.25°	39	Dufresne et al. (2013)
Max Planck Institute Earth System Model, low resolution (MPI-ESM-LR)	Max Planck Institute for Meteorology, Germany	1.9° × 1.9°	47	Jungclaus et al. (2006); Zanchettin et al. (2012)
Norwegian Earth System Model, version 1 (intermediate resolution) (NorESM1-M)	Norwegian Climate Center, Norway	2.5° × 1.9°	26	Zhang et al. (2012)
Geophysical Fluid Dynamics Laboratory Earth System Model with Modular Ocean Model 4 (MOM4) ocean component (ESM2M) (GFDL-ESM2M)	National Oceanic and Atmospheric Administration (NOAA) Geophysical Fluid Dynamics Laboratory	2.5° × 2.0°	24	Donner et al. (2011)
L'Institut Pierre-Simon Laplace Coupled Model, version 5, coupled with NEMO, low resolution (IPSL-CM5A-LR)	Institut Pierre Simon Laplace, France	3.75° × 1.8°	39	Dufresne et al. (2013)
Beijing Climate Center, Climate System Model, version 1.1 (BCC-CSM1.1)	Beijing Climate Center, China Meteorological Administration, China	2.8° × 2.8°	26	Wu et al. (2010)
Model for Interdisciplinary Research on Climate, Earth System Model, Chemistry Coupled (MIROC-ESM-CHEM)	Japan Agency for Marine-Earth Science and Technology	2.8° × 2.8°	80	Wantanabe et al. (2011)

points, like local minima in the field, within each object. The minima are identified by comparing each object point with its neighbors. If clusters of local minima occur with points having the same local extreme value, the centroid of these points is found for each cluster so that each cluster is represented by a single feature point. To determine the correspondence between the feature points, a constrained optimization of a cost function is

used (based on the algorithm of Salari and Sethi 1990). Those identified storms are filtered to retain only those that last at least 24 h and move farther than 1000 km over their lifetime. Hodges et al. (2011) used 48 h as a threshold, but we found it reduced the number of cyclones by ~15% and that 24 h performed best in our study region through a trial and error process.

The automated cyclone tracking was evaluated manually for 11 Januaries every other year from 1980 to 2000 from 20 to 60°N and 40 to 90°W. The cyclone needed to include at least a 2-hPa closed MSLP contour to be counted manually, and the storm had to persist for at least 24 h and move at least 1000 km, which are two criteria used for the automated tracking. There were 2286 cyclone centers identified during this period, with 181 cyclone centers missed (7.9%) and 103 false alarmed (4.5%) by the tracking. Therefore, the uncertainty of the automated cyclone tracking results is 5%–10%.

Other studies have used 850-hPa vorticity to obtain cyclone climatologies from global models (e.g., Hoskins and Hodges 2002; Anderson et al. 2003; Hodges et al. 2011). As in Hoskins and Hodges (2002), we spectrally filtered the data at T42 before tracking the cyclones using the 850-hPa vorticity, but we used a 24-h minimum cyclone lifetime rather than a 48-h lifetime as in Hodges' papers. However, there are 15%–20% more false alarm rates using 850-hPa vorticity than MSLP, since vorticity maxima are also collocated with elongated surface troughs rather than closed cyclone centers, as shown for 0600 UTC 10 January 2001 (Fig. 2). In contrast, the MSLP approach correctly identifies the well-defined cyclone over the western Atlantic at this time. There is a slight shift between the automated cyclone position and the actual MSLP pressure minimum, since the Hodges approach tracks pressure anomalies, not total pressure. As a result, to get the minimum MSLP for each cyclone, the lowest pressure within 5° of the identified pressure anomaly was applied. The number of cyclones identified using vorticity tracking is reduced if a 48-h lifetime is used (not shown), including eliminating the false alarms on 0600 UTC 10 January 2001; however, we found that too many observed cyclones are removed that have a lifetime between 24 and 48 h (not shown).

The 15 CMIP models in Table 1 are ordered from highest to lowest horizontal grid spatial resolution, since the seven highest-resolution members are compared with the eight lowest-resolution members in section 3 below. Each member, the CMIP5 mean, and the mean for the high- versus lower-resolution members were evaluated for cyclone track density and central pressure. For cyclone density, a spatial correlation of the track density (TR) of each member over the EC-WA box in Fig. 1 is computed with that based on the CFSR:

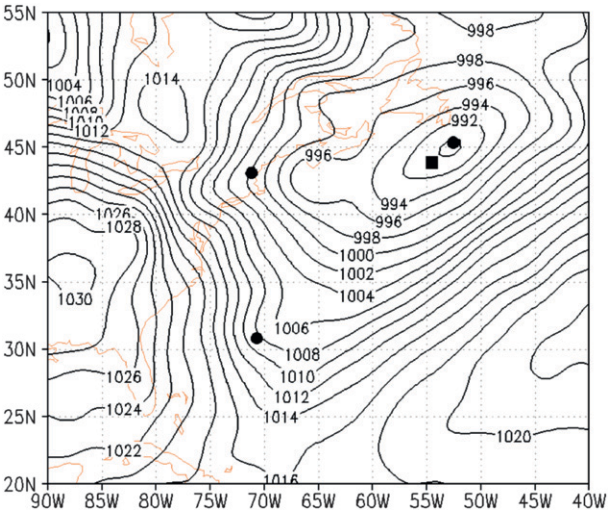

FIG. 2. Sea level pressure analysis (every 2 hPa) from the CFSR at 0600 UTC 10 Jan 2001. The dots and box represent where the vorticity and sea level tracking approaches identified cyclones, respectively, using the 24-h lifetime threshold. The sea level tracking is based on the anomaly of pressure, and therefore it does not necessarily lie exactly at the low center.

$$\mathrm{TR} = \frac{\sum_{i=0}^{n} (M_i - \overline{M})(C_i - \overline{C})}{\sqrt{\sum_{i=0}^{n} (M_i - \overline{M})^2} \sqrt{\sum_{i=0}^{n} (C_i - \overline{C})^2}}, \qquad (1)$$

in which M_i is the model track density for grid i, $\overline{M}$ is the model average track density of all grids, C_i is the CFSR track density in grid i, $\overline{C}$ is the CFSR average track density of all grids, and n is the number of total grids. A similar spatial correlation was also calculated for the distribution of cyclone central pressures [central pressure correlation (PR)], in which M_i is the model cyclone number in pressure bin i, $\overline{M}$ is the model average cyclone number of all bins, C_i is the CFSR cyclone number in bin i, $\overline{C}$ is the CFSR average cyclone number of all bins, and n is the number of total bins (n = 11; <935, 935–945, 945–955 … 1015–1025, and >1025 hPa).

An absolute difference was calculated for the track density absolute error (TD) within the EC-WA box in Fig. 1:

$$\mathrm{TD} = \frac{1}{n} \sum_{i=0}^{n} (|M_i - C_i|), \qquad (2)$$

in which M_i is the model track density in grid box i, C_i is the CFSR track density in grid i, and n is the total number of grids. A mean absolute difference of cyclone number for three pressure bins (PD) was also calculated using Eq. (2), in which M_i is the model cyclone number

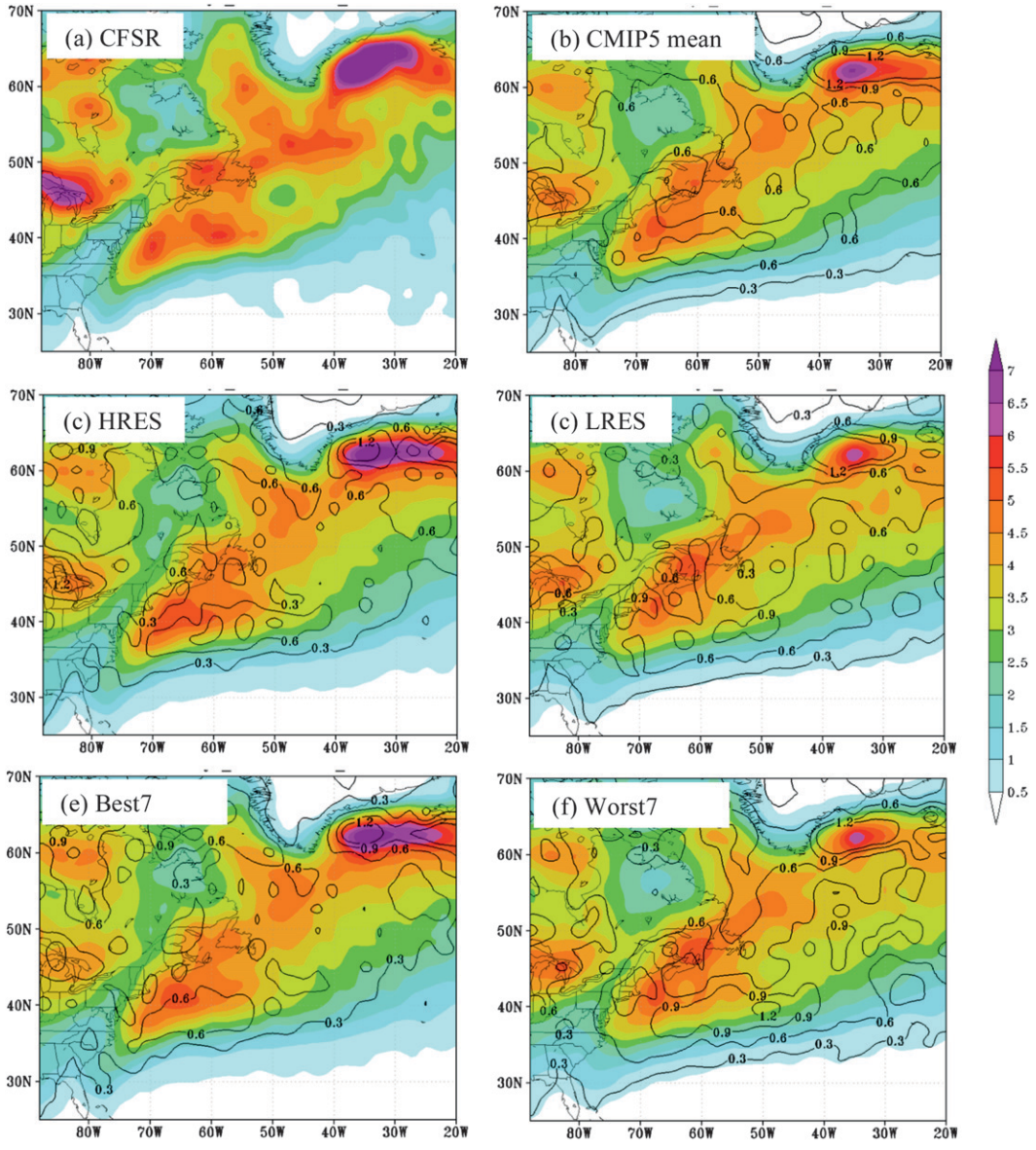

FIG. 3. (a) Cyclone track density for the CFSR analysis showing the number of cyclones per cool season (November–March) per 50 000 km^2 for 1979–2004. (b) As in (a), but for the mean (shaded) and spread (contoured every 0.3) of all CMIP5 models in Table 1. As in (b), but for the (c) high-resolution (HRES), (d) low-resolution (LRES), (e) Best7, and (f) Worst7 models.

in bin i, C_i is the CFSR cyclone number in bin i, and n is the total number of total bins ($n = 3$; <975, 975–1005, and >1005 hPa).

The historical evaluation and future changes of cyclones were diagnosed for three domains from eastern North America to the western Atlantic (cf. Fig. 1). The smaller East Coast domains are used to better understand the cyclone changes in this highly populated coastal region. An analysis of some of the reasons for select model differences is shown in section 3c.

3. CMIP5 cyclone predictions

a. Historical evaluations

The cyclone track density for the CMIP5 mean, mean of the seven high- versus eight lower-resolution members (gray and black members in Table 1, respectively), and selected individual members are compared with the CFSR for the cool seasons of 1979–2004. From eastern North America to the central Atlantic in the CFSR (Fig. 3a),

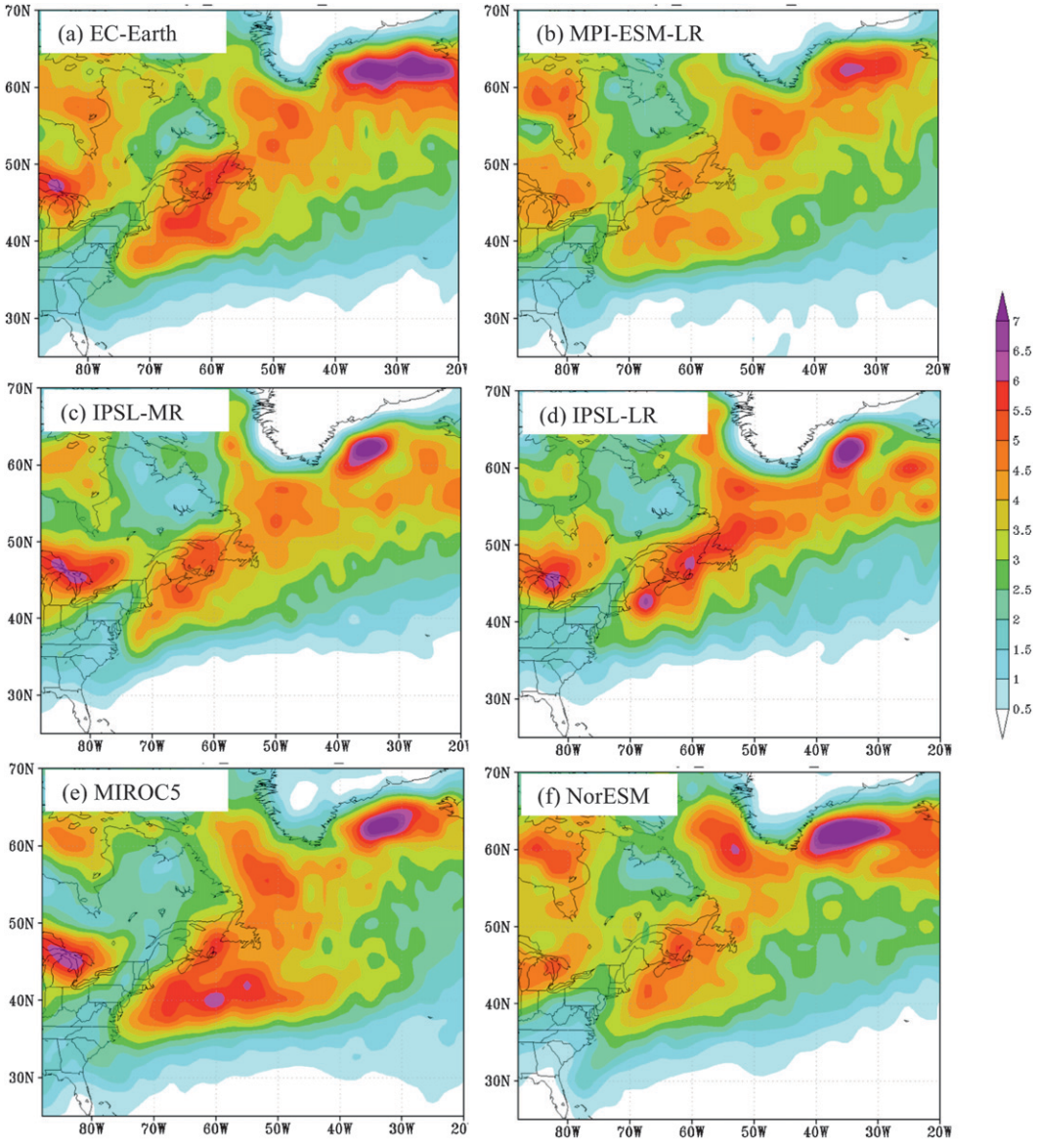

FIG. 4. As in Fig. 3, but for selected CMIP5 members (a) EC-Earth, (b) MPI-ESM-LR, (c) IPSL-MR, (d) IPSL-LR, (e) MIROC, and (f) NorESM.

there are three clusters of high cyclone track density (>5 cyclones per cool season per 50 000 km^2): around the Great Lakes, north of the Gulf Stream over the western Atlantic, and just east of southeast Greenland. The CMIP mean was able to realistically simulate these three maxima (Fig. 3b); however, the mean values are underpredicted by 10%–25%. There is also a relatively large spread (evaluated as one standard deviation) in the CMIP5 predictions in these regions (~1.0 cyclone per cool season per 50 000 km^2).

There are also some important differences in the climatology of historical cyclone densities between the seven highest-resolution members and the other eight members (Figs. 3c,d). The mean of the higher-resolution members has a more well-defined track maxima just north of the Gulf Stream and to the east of southern Greenland (difference significant at the 95% level), which is more similar to the CFSR than the lower-resolution members, which have the track density maximum too far north and close to the U.S. Northeast coast (also significant at the 95% level). This result is similar to Woollings et al. (2010), who found that using a higher SST resolution tended to shift the storm track southward toward the Gulf Stream.

Fig. 4 shows the historical (1979–2004) cyclone density for the cool season for the EC-Earth, MPI-ESM-LR,

IPSL-MR, IPSL-LR, MIROC5, and NorESM models in order to highlight some more of the model variability as well as some potential impact of model resolution. Sheffield et al. (2013) highlight some other CMIP5 models used in this analysis. The two higher-resolution members (EC-Earth and MIROC5) have a well-defined storm track that extends east-northeastward from the mid-Atlantic U.S. coast (Figs. 4a,e). The MIROC5 overpredicts the cyclone density and eastward extension of the maximum in this region (Fig. 4e), while the EC-Earth is more similar to the CFSR just north of the Gulf Stream (Fig. 4a). Two of the lower-resolution members (NorESM and IPSL-LR) have a storm track shifted too far north and close to the coast (Figs. 4d,f). However, even the relatively low-resolution IPSL-LR can produce a track density maximum (6–7) greater than the CFSR, while the MPI-ESM-LR has the cyclone track farther offshore of the coast as in the CFSR (Fig. 4b). These differences for models with similar resolutions illustrate that model setup/physics differences can be just as important as model spatial resolution.

A comparison of IPSL-LR and IPSL-MR highlights more of the impact of spatial resolution, since this was the only difference between these two members (Figs. 4c,d). A ~50% increase of the horizontal resolution in IPSL-MR reduces the near-coast maximum by 10%–20% just east of the Northeast U.S. coast and shifts the cyclone density farther southward along the U.S. East Coast, which is more similar to the CFSR.

The distribution of maximum cyclone intensities (minimum central pressure during lifetime) was obtained for all CMIP5 members, CMIP5 mean, seven highest resolution, and eight lowest resolution for all available cyclone tracks over a large portion of the western and central Atlantic (EC-WA box in Fig. 1) for the 1979–2004 cool seasons. The central pressures were separated into 10-hPa bins (Fig. 5). The CFSR has a maximum for the 995–1005-hPa bin, while most of the lower-resolution CMIP5 members peak around 985–995 hPa (Fig. 5a). The mean of these eight lower-resolution members is nearly equal to the CFSR, but these members underpredict the numbers in all categories except the 985–995 hPa. Overall, the distribution for the mean of these eight lower-resolution CMIP5 models is narrower than observed. Most of the seven higher-resolution members also underpredict the frequency of <970-hPa cyclones (Fig. 5b), except the MRI-GCM3. Interestingly, the MIROC5 overpredicts the cyclone frequency between 980 and 1010 hPa, but it underpredicts the number of cyclones for <970 hPa. The mean of the seven higher-resolution members does correctly represent the distribution of cyclones >980 hPa, including the peak around 995–1005 hPa. The spread in the cyclone number is about half as large for the seven higher-resolution members than the lower resolution. Overall, the frequency distribution for cyclone central pressure illustrates that the mean is often better than any one member or small subset of members, given the relatively large spread in cyclone predictions.

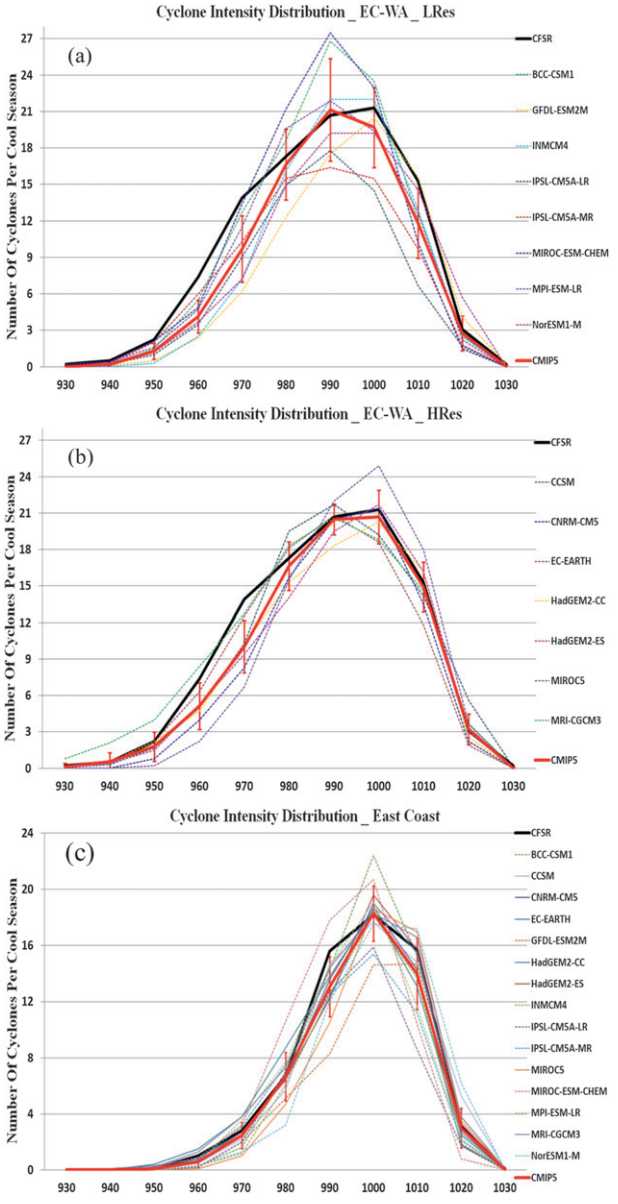

FIG. 5. Number of cyclone minimum central pressures per cool season for 1979–2004 within the EC-WA box region in Fig. 1 for a 10-hPa range centered every 10 hPa showing the CFSR (bold black), CMIP mean of the low-resolution models, and each of the low-resolution models. (b) As in (a), but for the higher-resolution CMIP5 models in Table 1. (c) As in (b), but for all CMIP models and for ECL and ECW boxes in Fig. 1.

TABLE 2. Verification of the CMIP5 models for TR, TD, PR, and PD. The CMIP5 member ranking is presented for each of these verification metrics, and the models are ordered according to their final ranking. The verification of the CMIP5 mean, Best7, high-resolution seven (HRes7), and low-resolution eight (LRes8) models is also presented, with the Hres7 in boldface.

Models	TR	TD	PR	PD	Rk-TR	Rk-TD	Rk-PR	Rk-PD
EC-EARTH	**0.9493**	**0.532**	**0.9889**	**3.13**	**1**	**4**	**2**	**3**
MRI-CGCM3	**0.9091**	**0.517**	**0.9920**	**1.90**	**9**	**2**	**1**	**1**
CNRM-CM5	**0.9415**	**0.513**	**0.9797**	**5.23**	**2**	**1**	**7**	**7**
MPI-ESM-LR	0.9404	0.553	0.9831	3.77	3	6	5	4
HadGEM2-ES	**0.9284**	**0.519**	**0.9812**	**4.10**	**6**	**3**	**6**	**6**
HadGEM2-CC	**0.9108**	**0.555**	**0.9873**	**4.03**	**8**	**7**	**4**	**5**
CCSM4	**0.9180**	**0.651**	**0.9759**	**3.07**	**7**	**11**	**9**	**2**
IPSL-CM5A-MR	0.9325	0.708	0.9879	8.20	4	12	3	13
BCC-CSM1	0.9035	0.544	0.9764	5.97	12	5	8	8
INM-CM4.0	0.9081	0.577	0.9631	6.07	11	8	10	9
GFDL-ESM2M	0.9307	0.588	0.9460	8.43	5	9	15	14
NorESM1	0.9089	0.747	0.9629	6.57	10	13	11	10
MIROC5	**0.8884**	**0.640**	**0.9469**	**7.10**	**14**	**10**	**14**	**11**
MIROC-ESM-CHEM	0.8839	0.783	0.9609	7.50	15	14	12	12
IPSL-CM5A-LR	0.8987	0.879	0.9594	10.93	13	15	13	15
Mean	0.9667	0.340	0.9868	3.67				
Best7	0.9634	0.352	0.9932	2.80				
HRes7	0.9614	0.358	0.9899	2.82				
LRes8	0.9580	0.379	0.9828	4.89				

Fig. 5c shows the distribution of cyclone maximum intensity (minimum central pressure) for the combined East Coast land and water areas (ECL and ECW boxes in Fig. 1). This central pressure distribution near the entrance of the storm track is narrower than the larger western Atlantic domain. The mean of the CMIP5 models better depicts this East Coast distribution than the larger Atlantic domain, with less underprediction for relatively deep or weak cyclones. The largest spread is associated with several of the lower-resolution models, with many members either underpredicting or overpredicting the peak number around 1000 hPa.

Table 2 presents the validation within the EC-WA box region in Fig. 1 for the individual 15 CMIP5 members, the mean of all CMIP5 members, seven highest-resolution members, eight lowest-resolution members, and the seven best members (hereafter referred to as Best7). As described in section 2, the TR and PR were calculated as well as the TD and PD. The 15 CMIP5 models are ranked separately for each of these metrics, and a combined (overall) rank is obtained by averaging the ranks for TR, PR, TD, and PD, which is shown by the order of models listed in Table 2. For cyclone density, the TR (TD) scores range from 0.949 (0.53) for the EC-Earth to 0.899 (0.88) for the IPSL-LR model. The EC-Earth model has the best track density, since it best captures the position and number of tracks (Figs. 3a, 4a), while the IPSL-LR is ranked last given its northward shift of the storm track and maximum too close to the coast (Fig. 4d). Most of the top seven models for track density are also in the top seven for cyclone intensity. However, the GFDL-ESM2M is the fifth best for track density but 14–15th for intensity, while the MRI-CGCM3 is the ninth for density and first for intensity. The PD ranged from 1.9 for the MRI-CGCM3 to 10.9 for the IPSL-LR. For the final ranking, six of the top seven models were the top seven higher-resolution models, so increasing resolution improves most of the predictions. However, there are exceptions since the lower-resolution MPI-ESM-LR is ranked fourth overall, while the relatively high-resolution MIROC5 is ranked third from the bottom.

For cyclone track density, the mean of all CMIP members has the best TR and TD scores, while the Best7 and seven higher-resolution members have smaller errors than the overall mean for cyclone intensity, since some outliers increase the error for the overall mean. The only CMIP5 member that has less error for central pressure than the Best7 is the MRI-CGM3. Although the overall CMIP5 mean is best for cyclone density, the Best7 statistics will be highlighted below for most metrics, since it has lower errors than CMIP5 mean for intensity. A seven worst members (Worst7) category is also defined and used below, which includes those members that finished in the bottom seven of the verification ranking (Table 2).

Figure 6 shows a comparison of the cyclogenesis density locations for the historical period between the CFSR, CMIP5 mean, Best7, and Worst7. Most cyclogenesis events, which are defined as the first point in the cyclone track, occur just offshore of the U.S. East Coast

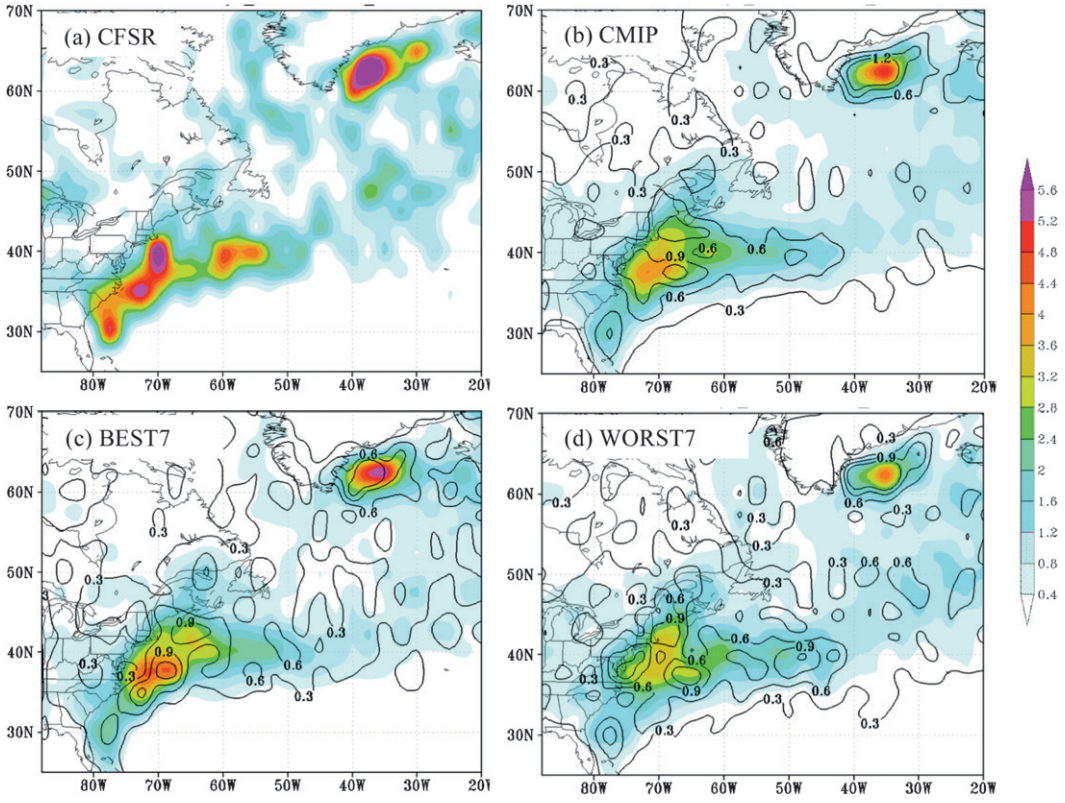

FIG. 6. Cyclogenesis density (number per 5 cool seasons per 50 000 km^2) for the historical 1979–2004 period for the (a) CFSR, as well as the mean and spread for (b) all CMIP members, (c) Best7 members, and (d) Worst7 members.

in the CFSR, with 3–6 cyclones per five cool seasons per 50 000 km^2. Another maximum of similar amplitude is located just east of southeast Greenland. The CMIP5 mean and Best7 have a similar structure as the CFSR, but both underestimate the genesis along the U.S. East Coast by 10%–20% to the north and 40%–50% to the south. The Best7 is slightly better than the CMIP mean, since the Best7 has 5%–10% more genesis along the East Coast. In contrast, the Worst7 underestimates the genesis density by a nearly a factor of 2 just east of the mid-Atlantic and Northeast U.S. coasts. The better result for the Best7, which primarily includes the higher-resolution CMIP5 models, reiterates the importance of spatial resolution to more accurately predict cyclogenesis for this western Atlantic region.

The 6-h cyclone central pressure deepening rates were also compared between the CMIP mean, Best7, and Worst7 members for the western Atlantic and smaller East Coast domains (Fig. 7). For both regions, the Worst7 underpredicts the more rapidly deepening [from -10 to -6 hPa (6 h)$^{-1}$] deepening rates, while the Best7 is most similar to the CFSR, with the Best7 distribution nearly equal to the CFSR for the East Coast domains for these more rapidly deepening storms. Meanwhile, the Worst7 overpredicts the number of cases experiencing little or no deepening than the Best7. The CFSR maximum [>5 hPa (6 h)$^{-1}$] is located several hundred kilometers to the east of the Northeast U.S. coast and to the northeast of Newfoundland (Fig. 8a). The Best7 mean has both of these maxima (Fig. 8d), but they are underpredicted by 20%–30% (Fig. 8b), while the Worst7 underestimates by nearly a factor of 2 (Fig. 8c).

Fig. 9a shows a time series of the number of cyclones per cool season within the EC_WA box in Fig. 1. There was an upward trend in cyclones in the CFSR between 1979 and 1991 (10%–15% increase), but there has been a slight downward trend since the early 1990s (5%–10%). There is a slight (~5%) decline in the CMIP mean since the early 1990s, which is most pronounced in the Worst7 mean. The Best7 better simulates the number of cyclones compared to the CMIP5 and Worst7 means, but all means underpredict storms and there is a relatively large (30%–40%) spread in the number of cyclones among the models.

b. *Future projections*

The CMIP5 models were evaluated to diagnose potential future changes in cyclone track density, intensity,

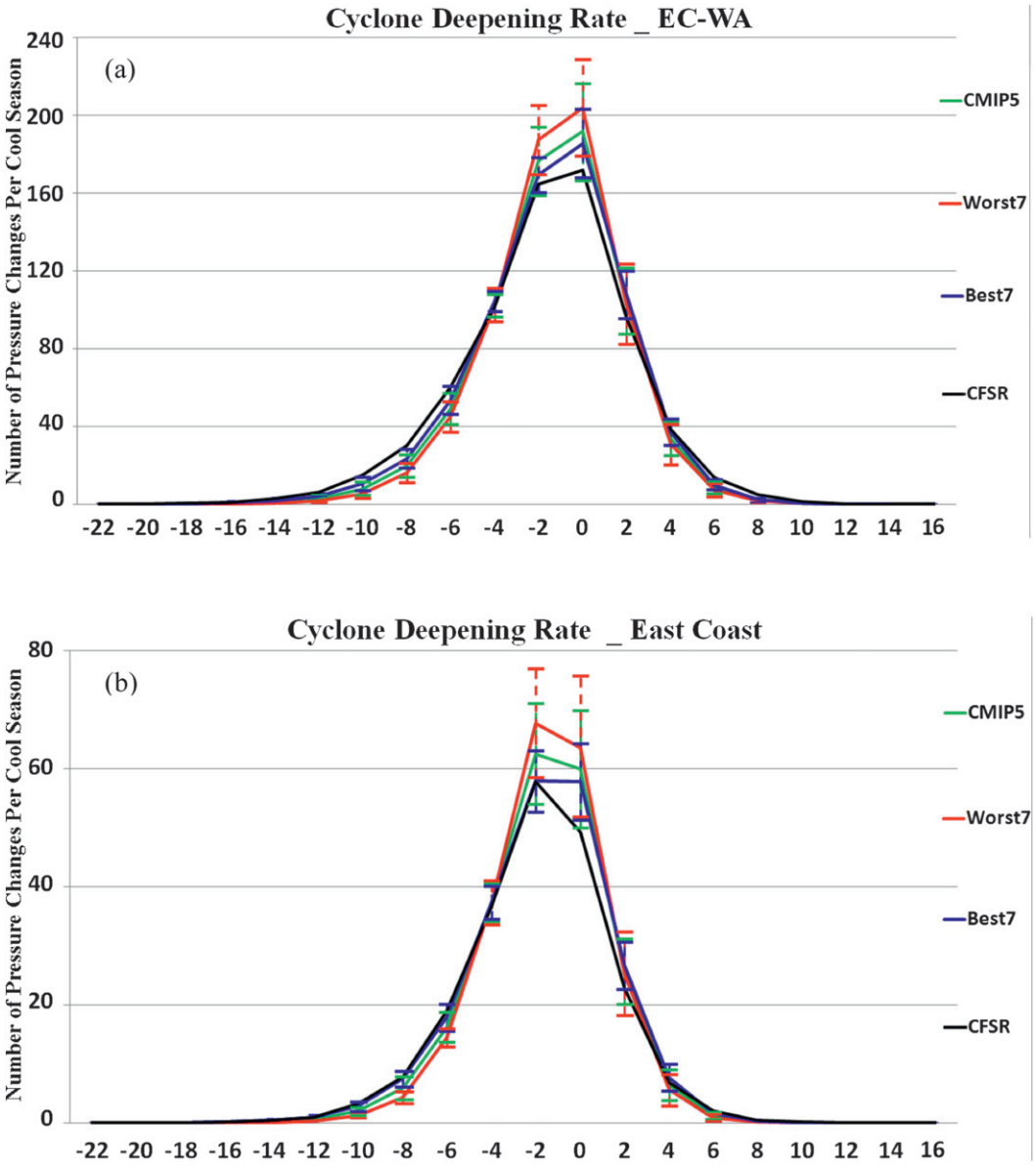

FIG. 7. (a) Number and spread (one standard deviation range given by the vertical bar) of 6-h cyclone central pressure changes per cool season for the 1979–2004 period over the western Atlantic domain for the CFSR, CMIP mean, Best7, and Worst7 models. (b) As in (a), but for the combined ECL and ECW box domains.

and deepening rates. Emphasis will be put on the Best7 models, since these models better represented the cyclones during the historical period. Fig. 10 shows the change in cyclone track density over the northern Atlantic for three future periods (2009–38, 2039–68, and 2069–98) as compared to the historical period. All the dotted areas on the future plots have at least 6/7 (85%) of the Best7 members agreeing in the sign of the future cyclone change. For 2009–38 (Fig. 10a), there is a 0.2–0.8 (5%–10%) reduction in cyclone density over areas of the western Atlantic near the Gulf Stream in the Best7 models. Meanwhile, there was a 5%–10% increase in track density around Nova Scotia in southeast Canada. There was less indication of track changes in the Worst7 models during this period (not shown). Over the western Atlantic, the cyclone density reduction increases in magnitude (to 10%–15%) and spatial extent during the mid-twenty-first century (2039–68) in the Best7 models (Fig. 10b). By the late-twenty-first century (Fig. 10c), there are 15%–20% fewer cyclones over much of the western Atlantic storm track and to the east of southern Greenland. Meanwhile, there was a 5%–10% increase

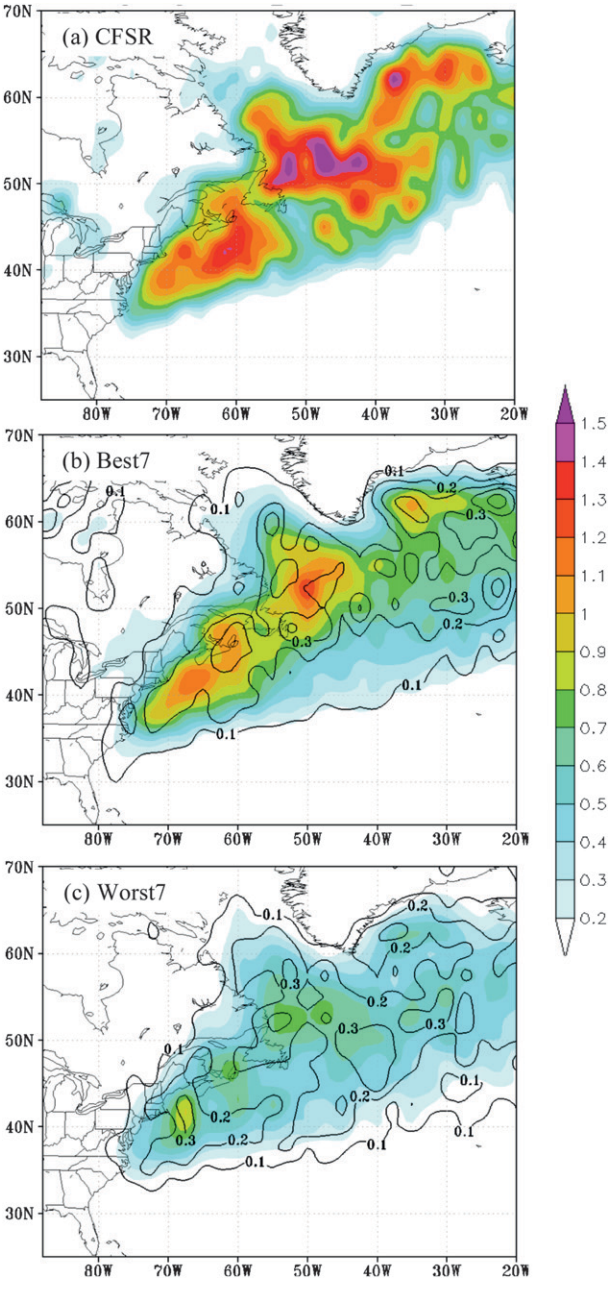

FIG. 8. Spatial density of deepening rates >5 hPa $(6\,h)^{-1}$ averaged for all historical cool seasons per 50 000 km^2 for the (a) CFSR, (b) Best7, and (c) Worst7.

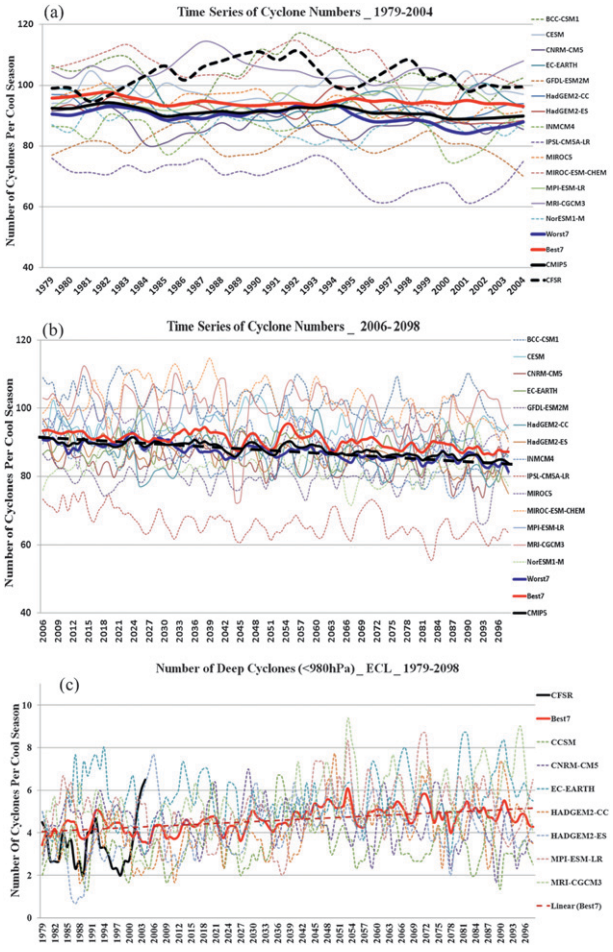

FIG. 9. (a) Time series for the 1979–2004 cool seasons showing the numbers of cyclones per cool season within the EC-WA box in Fig. 1 for the CFSR, mean of all CMIP5 members, Best7, Worst7, and individual members (Best7 members solid and Worst7 dashed). (b) As in (a), but for the 2006–98 period and a linear fit (dashed) is made for the CMIP5 mean (black). (c) As in (a), but for the number of relatively deep cyclones (<980 hPa) for Best7 models and mean in the ECL region for the 1979–2098 period.

along the U.S. coast and 10%–20% increases along the eastern Canadian coast. For this same period, the Worst7 changes relative to the historical period are 5%–10% less than the Best7 along the coast of eastern North America and the western Atlantic (Fig. 10d). Also, there is little change in the cyclone density in the Worst7 over southeast Canada between the historical and late-twenty-first century.

After averaging all the CMIP5 members over the EC-WA box, there is a near-linear decrease in cyclone frequency in the CMIP5 mean of around seven cyclones per cool season over the 2009–98 period (Fig. 9b), and this trend is similar between Best7 and Worst7 groupings when averaged for this box. There is also a large spread in the cyclone number in the CMIP models over the twenty-first century, ranging from 60 to 70 cyclones per cool season in the IPSL to 100–110 in the MIROC-ESM and BCC-CSM. However, all models trend downward in cyclone number, with two-thirds of the models (and CMIP mean, Best7, and Worst7) having a nonzero trend that is significant at least at the 90% confidence level using an F test.

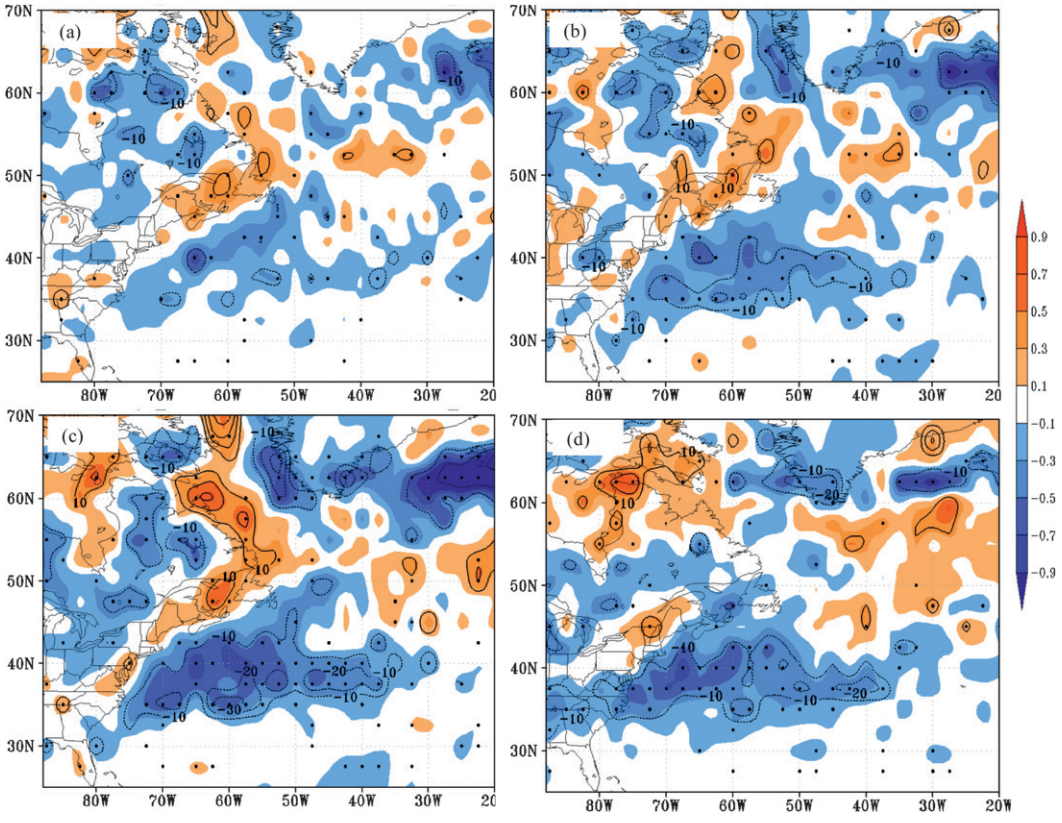

FIG. 10. Difference in cyclone track density (shaded per cool season per 50 000 km^2) for the Best7 mean between the (a) 2009–38, (b) 2039–68, and (c) 2069–98 cool seasons and the historical (1979–2004) and percent change (contoured every 10%). The dots are locations in which six of the seven Best7 models agree with the sign of the change. (d) As in (c), but for Worst7.

Fig. 11 shows the difference and spread averaged for the Best7 models in the number of cyclones attaining a maximum intensity (minimum pressure) within each 10-hPa intensity bin for the domains in Fig. 1 for the three future twenty-first-century periods. For the larger EC-WA domain (Figs. 11a,b), most of the cyclone reduction (3%–6%) is for the relatively weak (1010–1020 hPa) cyclones, and this reduction nearly doubles from the early–late-twenty-first century, with the spread of models within one standard deviation of the mean for 1005–1015 hPa, all indicating weakening. The Worst7 models have nearly twice as large of a reduction for these weaker cyclones by the later twenty-first century (not shown). The number of relatively deep cyclones (<980 hPa) also decreases 3%–10%, with the mean of the Best7 models indicating less frequent storms around 970 hPa. In contrast, for the ECL there is a 5%–40% increase in the number of 960–980-hPa cyclones by the mid-twenty-first century (Figs. 11c,d) with generally good model agreement (low spread), but the trend reverses slightly for the later twenty-first century. Fig. 9c shows a time series of this trend of the number of <980-hPa cyclones in the ECL, in which the peak number in the Best7 mean is reached by the 2050s. In contrast, there is little increase in these relatively strong cyclones for the ECW region (Figs. 11e,f). The reduction of relatively weak (1000–1020 hPa) cyclones for both ECL and ECW boxes ranges from 5% to 8% (0.7–0.9 cyclones per season) in the early twenty-first century to 10%–15% (−2.0 cyclones per season) in the later twenty-first century. Overall, these results suggest large spatial differences in how the intensity of cyclones will change between the entrance of the storm track (U.S. East Coast) to the middle of the storm track, as well as just inland and offshore of the U.S. East Coast.

The change in the frequency of the 6-h deepening rate of the cyclones was also calculated for each of the three future periods minus the historical period (Fig. 12). For the EC-WA domain (Figs. 12a,b), there was a reduction in the frequency of most of the deepening rates for all future periods. The largest changes between the −2 and −5 hPa (6 h)$^{-1}$ bins range from 2% to 4% in the early twenty-first century to 10%–15%

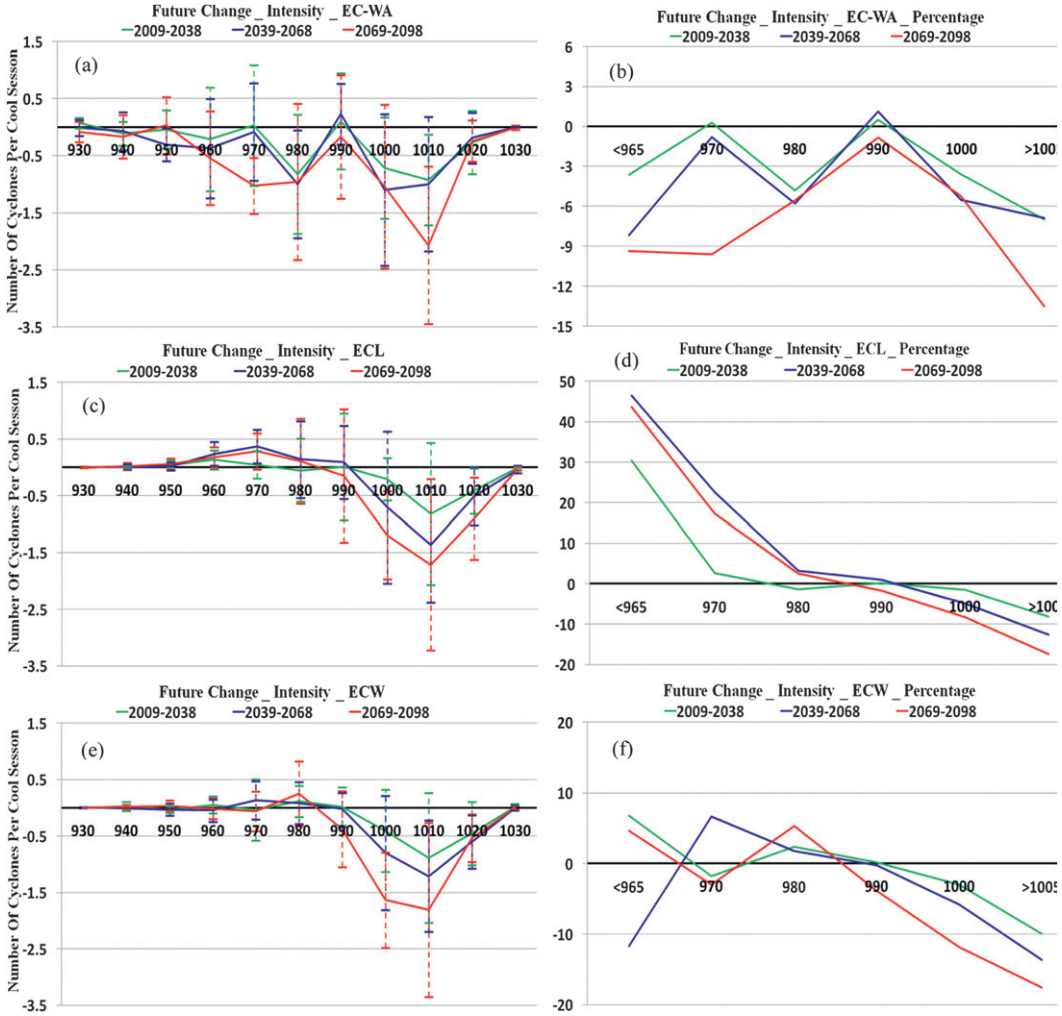

FIG. 11. Difference in the number of cyclones per cool season reaching their maximum intensity (minimum pressure) for each 10-hPa bin between the three future periods and 1979–2004 cool season for the (a) EC-WA, (c) ECL, and (e) ECW boxes in Fig. 1. The difference for each future period is for the mean of the results of each Best7 model, with the one standard deviation range shown by the vertical bar. (b) As in (a), but for percentage change. (d) As in (c), but for percentage change. (f) As in (e), but for except percentage change.

by the late-twenty-first century, with the spread indicating most models have this weakening by the late-twenty-first century. Meanwhile, there was little change in the 6-h weakening rate (filling) of cyclones between the 0 and 4 hPa $(6\,\mathrm{h})^{-1}$ bins. In contrast, for the ECL region there is a 0.5–1.0 (10%–35%) increase in the number of -4 to -10 hPa $(6\,\mathrm{h})^{-1}$ bins by the mid-twentieth century (Figs. 12c,d) and a 5%–10% increase by the late-twenty-first century. Meanwhile, any deepening increases (~5%) over the ECW region are limited to the early twenty-first century (Figs. 12e,f). The change in weakening rates for the ECL and ECW boxes are less than 5% for most pressure bins.

Fig. 13 shows the spatial change in the frequency of 6-h cyclone deepening rates >5 hPa between the three future periods for the Best7. During the early twenty-first century (Fig. 13a), there is a 5%–40% increase in this frequency over much of the Northeast United States, eastern Great Lakes, and southeast Canada, while there is a slight decrease (0%–20%) in this frequency over the western Atlantic storm track. By the mid-twenty-first century (2038–69; Fig. 13b), there is more widespread increase over the Northeast United States (10%–30%) and decrease (10%–20%) over the western Atlantic. By the late-twenty-first century, the cyclone deepening frequency increases are reduced as compared to the mid-twenty-first century, while there is a widespread 10%–30% decrease in 6-h deepening >5 hPa over much of the western and northern Atlantic.

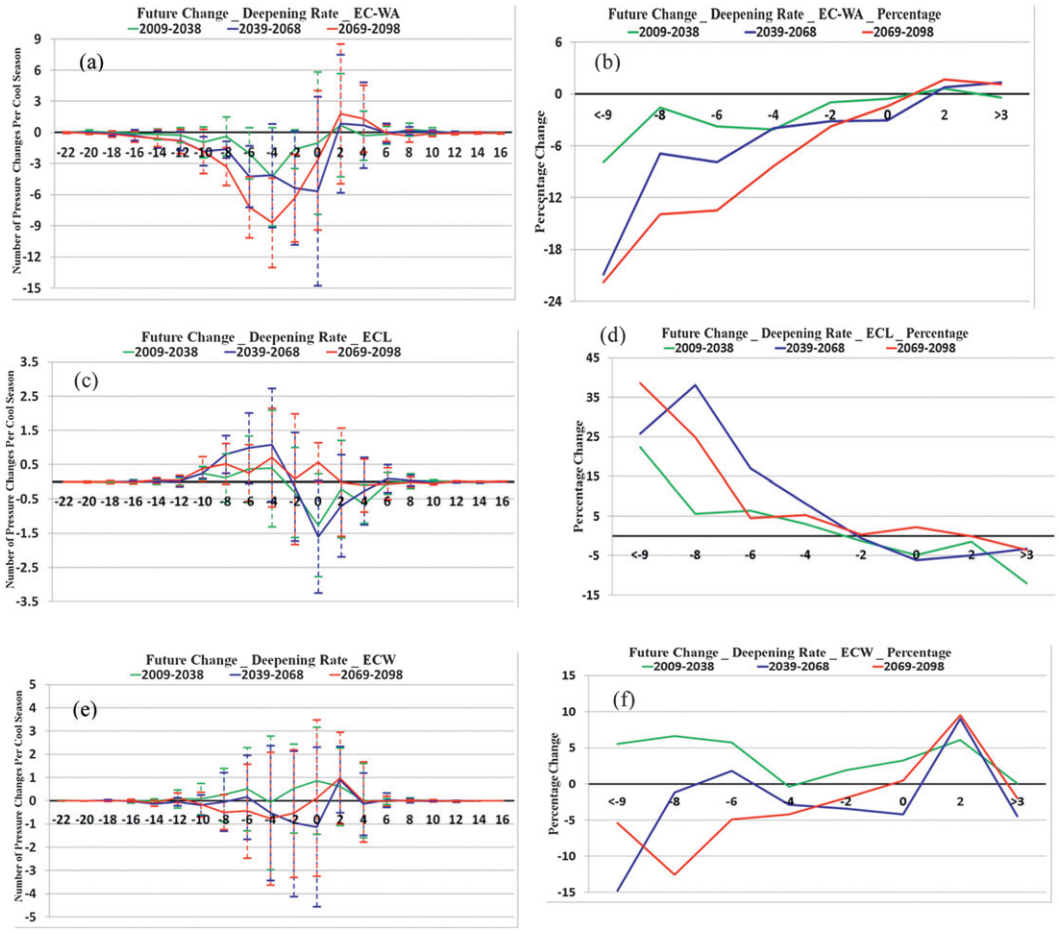

FIG. 12. As in Fig. 11, but for 6-h central pressure changes of the full cyclone evolution within the boxes (a),(b) EC-WA, (c),(d) ECL, and (e),(f) ECW for the three future periods minus the historical period. The dots are locations in which six of the seven Best7 models agree with the sign of the change.

The change in 850-hPa maximum winds around the cyclones in the ECL region between the past and future was also explored for two of the Best7 models (MPI-ESM-LR and MRI-CGCM3), since their 850-hPa wind data were easily accessible. For each cyclone time within the ECL region, the maximum 850-hPa wind within 10° of the cyclone center was recorded, and a distribution of these maximum winds was obtained for the historical and future periods. For the historical period (Fig. 14a), both models have a maximum frequency between 22 and 28 m s^{-1}, with the MPI-ESM-LR having more moderate wind events (16–28 m s^{-1}) and the MRI-CGCM3 having stronger wind events (>34 m s^{-1}). For the future periods (Figs. 14b,c), there is a 10%–20% reduction in the number of 16–22 m s^{-1} wind events for the 2039–68 and 2069–98 periods, while there is a 15%–45% increase in the >34 m s^{-1} events. This suggests that for these two models there is a shift toward more intense cyclones by the mid-twenty-first century.

c. *Evaluation of model differences and future changes*

To understand some of the future cyclone changes in the models, the CMIP5 analysis also included averages of the daily near-surface (2 m) temperature gradient, 250-hPa wind speed, and Eady growth rate (Hoskins and Valdes 1990; Paciorek et al. 2002). The Eady growth rate is defined as

$$\sigma = 0.31 \frac{f}{N} \left| \frac{\partial \mathbf{V}}{\partial z} \right|, \tag{3}$$

where f is the Coriolis parameter, N is the buoyancy frequency, $\mathbf{V}$ is the horizontal wind vector, and z is the distance in the vertical. The Eady growth rate was calculated using daily data over the 850–500-hPa layer and then averaged for a set of cool seasons. Simmonds and Lim (2009) suggested that calculating the Eady growth rate from shorter time periods (daily or 6-h data) and

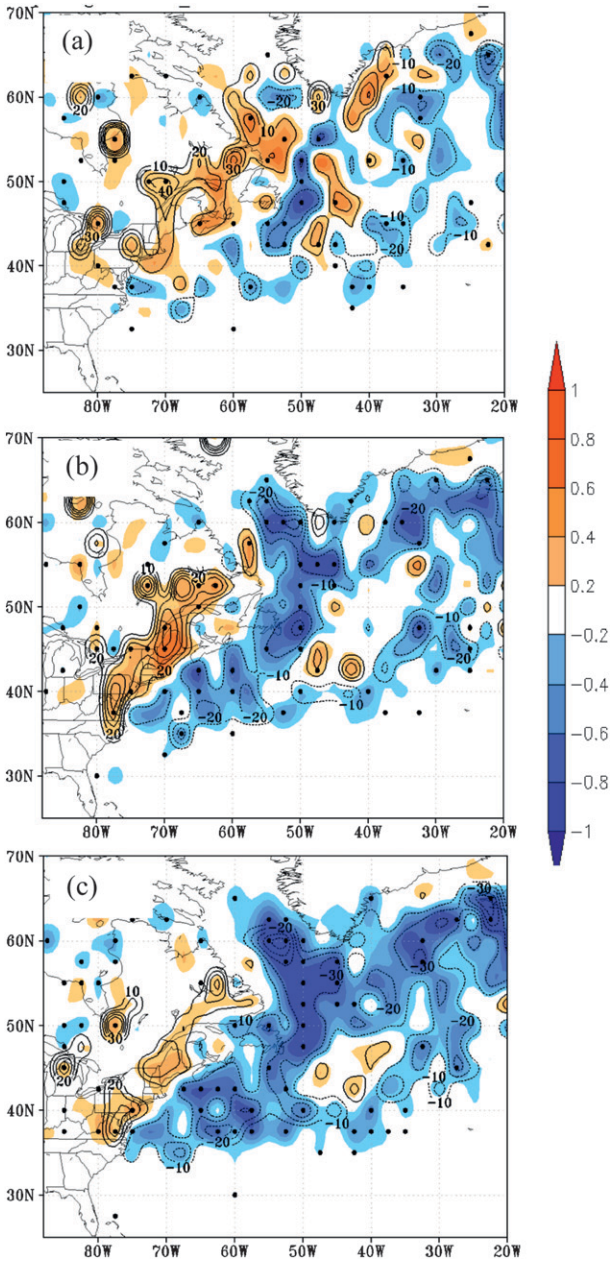

FIG. 13. Change in the number of 6-h cyclone deepening rates >5 hPa (shaded as the number of cyclone tracks per 5 cool seasons per 50 000 km^2) and the percentage change (contour every 10% with negative dashed) between the (a) 2009 and 2038, (b) 2039 and 2068, and (c) 2069 and 2098 future periods minus the 1979–2004 historical period.

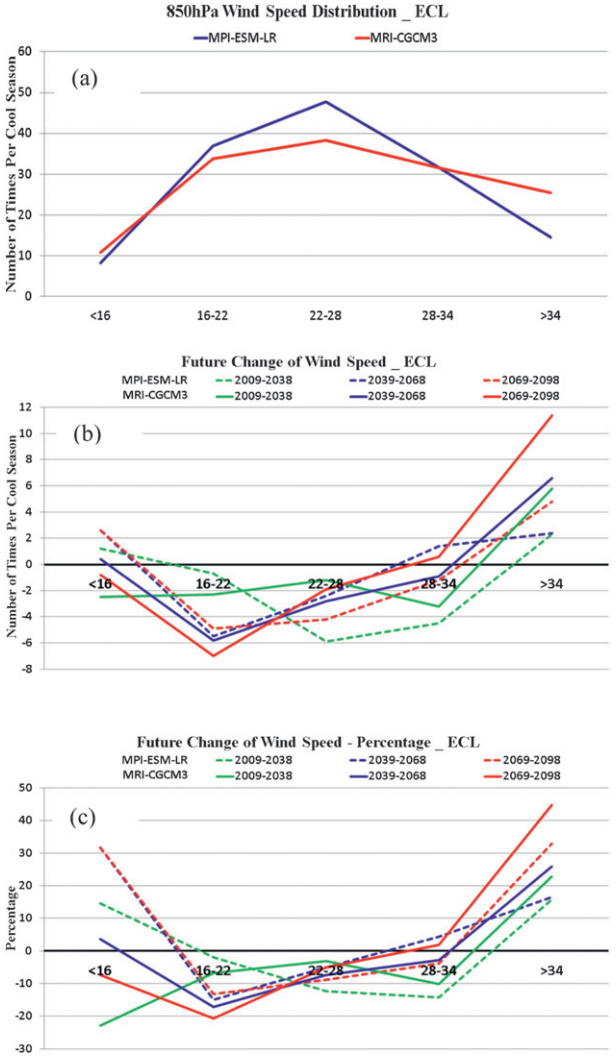

FIG. 14. (a) The number of times per cool season with the maximum 850-hPa wind speed within 10° around the cyclone falling within the specified bins (m s^{-1}) using only those cyclones within the ECL region for the MPI-ESM-LR and MRI-CGCM3 models for the historical (1979–2004) period. (b) As in (a), but for the change in number of occurrence between the three future periods and the historical. (c) As in (b), but for percent change.

then averaging these fields is better than calculating using monthly-mean data when drawing connections between changes in Eady growth and changes in cyclone properties.

The Eady growth rate and other variables were evaluated for the relatively high-resolution CNRM-CM5 and MIROC5 members, as well as the more coarse-resolution MPI-ESM-LR and IPSL-CM5A-LR models. The CFSR was used to compare the past performance of the Eady growth rate and other parameters with these four CMIP5 members. The models selected were based on data availability as well as their relative performance and resolution. Two relatively good performing models (CNRM-CM5 and MPI-ESM-LR) in Table 2 were contrasted with two models verifying in the bottom one-third (MIROC5 and IPSL-LR). Meanwhile, these same models also help compare differences between two relatively high-resolution models (MIROC5 and CNRM-CM5)

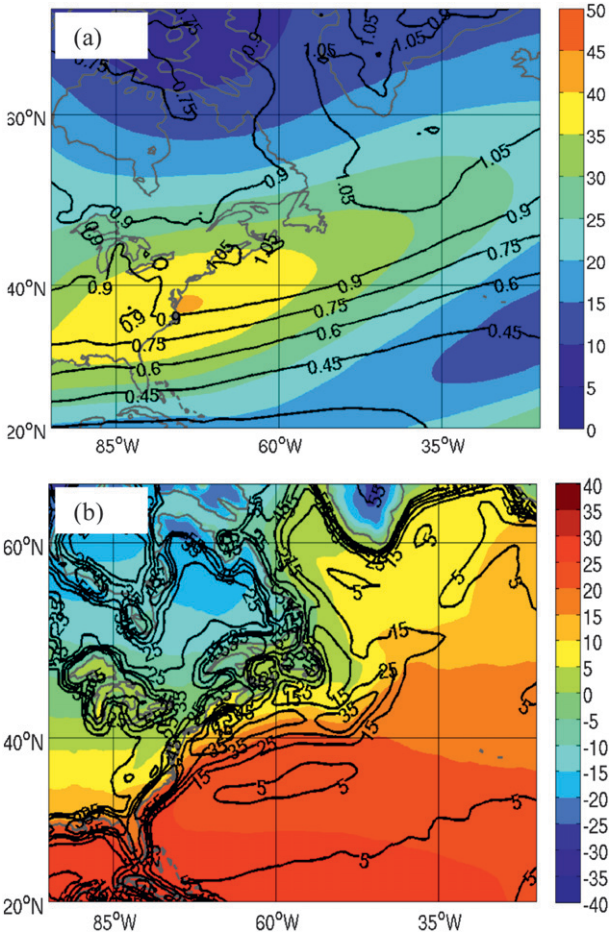

FIG. 15. (a) Average Eady growth rate (solid every 0.15 day^{-1}) and 250-hPa wind speeds (color shaded every 5 m s^{-1}) for the CFSR during the 1979–2004 cool seasons. (b) As in (a), but for the CFSR surface (2 m) temperature (color shaded every 5°C) and magnitude of the surface temperature gradient (solid every 5°C 1000 km^{-1}).

and lower-resolution models (MPI-ESM-LR and IPSL-LR).

The CFSR has an Eady growth rate maximum just east of the U.S. East Coast of around 1.05 day^{-1} and jet magnitude of 40 m s^{-1} (Figs. 15a,b). The model with the coarsest resolution and poorest cyclone performance (IPSL-LR) has the strongest upper-level jet (~47 m s^{-1}) and a relatively large Eady growth rate area of a >0.9 day^{-1} compared to the other four CMIP models over the western Atlantic (Fig. 16). Meanwhile, the other coarse-resolution model (MPI-ESM-LR) has a weaker ~37 m s^{-1} jet at 250 hPa and smaller area of a >0.9 day^{-1} Eady growth rate (Fig. 16b). Therefore, the relatively poor IPSL-LR performance was not the result of the lack of tropospheric baroclinicity as compared to the other models. Also, the excessive cyclone track density over the western Atlantic for the MIROC5 (cf. Figs. 3a, 4e) was not the result of an excessive Eady growth rate (Fig. 16c); however, its Eady maximum is farther south and the jet is more zonally elongated than the CFSR and other models.

The upper-level jet orientation and maximum were shifted ~500 km to the north in the two coarser-resolution members (MPI-LR and IPSL-LR) than the MIROC and CNRM-CM5, which suggests that there are vertical levels with different horizontal temperature gradients between the two sets of models. One important level for cyclogenesis is near the surface, which is impacted by the SSTs. Fig. 17 shows the 2-m temperature and absolute temperature gradient from the four CMIP models, which can be compared with the CFSR (Fig. 15b). All models except the IPSL-LR have the largest surface temperature gradient extending along the southeastern U.S. East Coast. The largest gradient in the IPSL-LR is farther north along the mid-Atlantic and Northeast U.S. coasts (Fig. 17d), which are where its cyclone density maximum was located (cf. Fig. 4d). The MPI-ESM-LR has the largest surface temperature gradient along the north side of the Gulf Stream (Figs. 17b,c), which is consistent with their more zonal elongation of the storm track. Only the MIROC5 realistically simulated the more southwest-to-northeast orientation of the surface temperature gradient to the east of 50°W. Chang et al. (2013) noted that the axis of the storm track tended to extend too zonally over the northern Atlantic, and Woollings et al. (2012) showed that nearly half of the northern Atlantic storm-track differences in the CMIP5 models were related to ocean circulation differences, so future work needs to investigate the role of the ocean coupling and SSTs in this bias.

We investigated the changes in the Eady growth rate and 250-hPa wind speeds between the historical and late-twenty-first century for the CRNM-CM5 and MIROC5 models (Figs. 18a,b). Consistent with the decrease in the western Atlantic cyclone density, there is a 5%–11% decrease (from −0.05 to −0.1 day^{-1}) in the Eady growth rate over eastern North America and the western Atlantic. The decrease in baroclinicity also results in a 2–6 m s^{-1} weaker upper-level jet, especially over eastern North America.

We also investigated some of the potential reasons for the slight increase in the number and intensity of storms just inland of the U.S. East Coast, especially during the mid-twenty-first century (Fig. 9c). Most of the analysis was restricted to the CCSM4 and MRI-CGCM3, since they were one of the Best7 models with either the largest positive cyclone density or intensity change over the ECL region. For the CCSM4, there was little change in

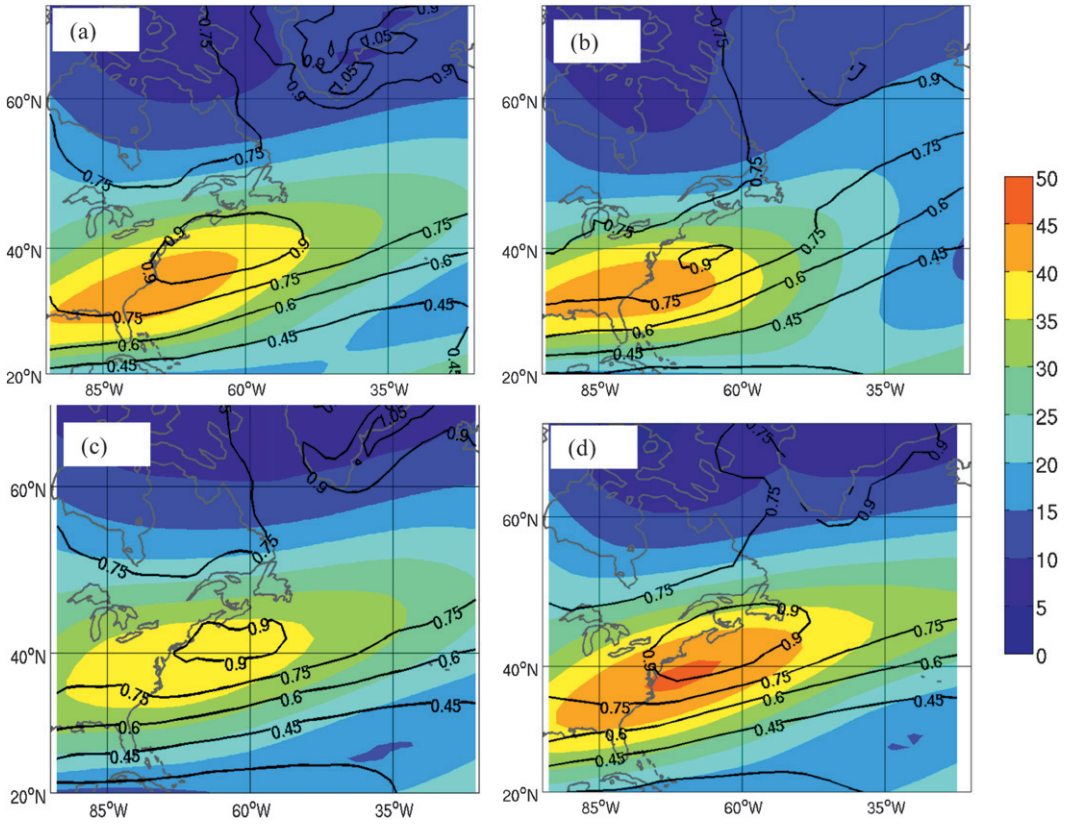

FIG. 16. As in Fig. 15a, but for the (a) CNRM-CM5, (b) MIROC5, (c) MPI-ESM-LR, and (d) IPSL-LR.

the 250-hPa windspeeds and Eady growth rate (Fig. 19a), and there was a slight decrease in the surface temperature gradient around the U.S. East Coast for the mid-twenty-first century (Fig. 19b). However, there was a 40–120-mm increase (10%–30%) of precipitation over this western region of the eastern U.S. storm track (Fig. 19c). The results from the MRI-CGCM3 were similar (not shown), although the precipitation increase over the eastern United States was somewhat less (10%–15%). These results suggest that there may be additional latent heating contributing to the slight enhancement of the number and intensity of surface cyclones even as the low-level temperature gradients along the coast weaken slightly during the twenty-first century. Future work needs to more carefully analyze the differences between the CMIP models to explain the differences in their future cyclone predictions.

4. Discussion and conclusions

This study has focused on the historical (1979–2004) evaluation and future projections of cool-season extratropical cyclone predictions within 15 CMIP5 models (Table 1) over eastern North America as well as the western and central North Atlantic. Mean sea level pressure (MSLP) every 6 h was used to track these cyclones using the Hodges (1994, 1995) tracking approach.

The CMIP5 extratropical cyclones for the historical period were evaluated for track density and cyclone central pressure (intensity) over eastern North America and the western Atlantic using the CFSR as the observational analysis. The 15 CMIP5 members were ranked given their density, intensity, and overall performance and these results were related to their resolution. Most of the seven lowest-resolution members have grid spacings of more than 2° in either the west–east or north–south directions. It was found that six of the top seven CMIP5 models with the highest spatial resolution were ranked the best overall. Higher-resolution members, such as MIROC5 and EC-Earth, tend to have a storm track that extends east-northeastward from the U.S. mid-Atlantic coast, while some of the lower-resolution members (NorESM and IPSL-LR) have the storms too far north and close to the coast. However, there are exceptions, such as the relatively low-resolution MPI-ESM-LR, which ranked number three for track density correlation over the western Atlantic. The higher-resolution CMIP5 models also better predicted the

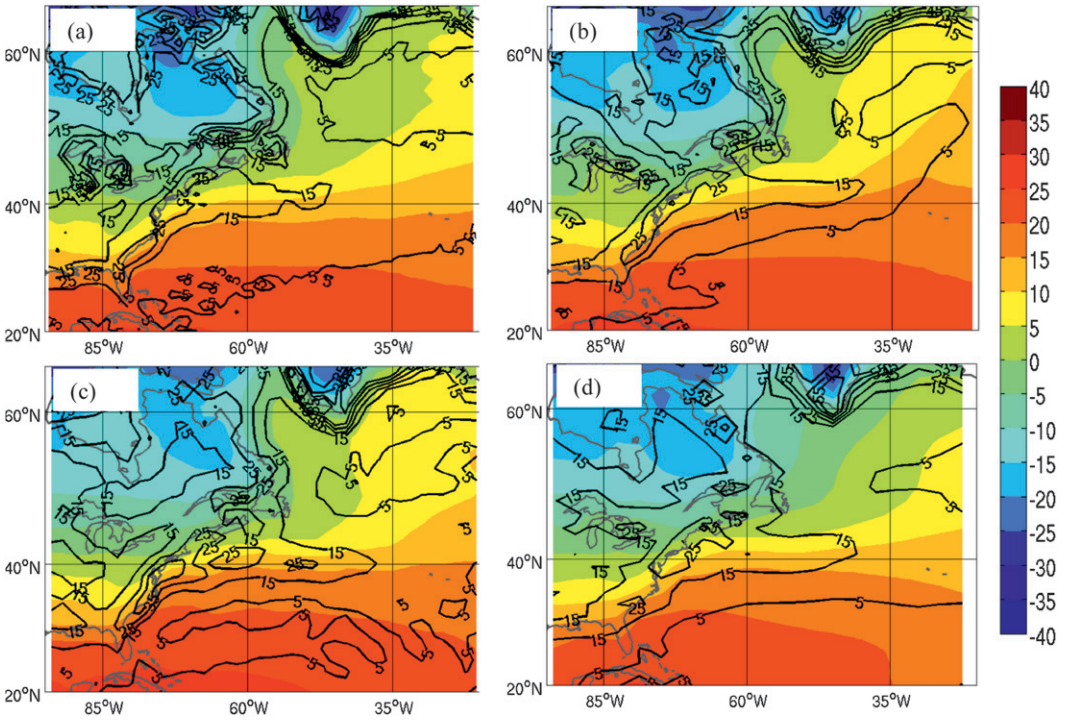

FIG. 17. As in Fig. 14b, but for the (a) CNRM-CM5, (b) MIROC5, (c) MPI-ESM-LR, and (d) IPSL-LR.

maximum intensity of these cyclones, since the eight lower-resolution models have a central pressure distribution that is too narrow (too few deep and weak cyclones). Even the higher-resolution CMIP5 models underpredict the relatively deep cyclones (<970 hPa) over the western and central North Atlantic, but they had little bias for these strong storms for a box around the U.S. East Coast. Overall, these results illustrate the importance of resolution in GCMs in realistically simulating the storm track. However, there were exceptions, which are consistent with Chang et al. (2013), who only found a −0.51 correlation between the storm-track amplitude in the CMIP3 models and model resolution in the Northern Hemisphere. Thus, resolution is not the only factor controlling storm-track amplitudes for some of these models.

Given the relatively poor cyclone density and intensity results for some of the CMIP5 members, we primarily utilized those CMIP models with the smallest track density and central pressure errors (Best7 models) to do the future change analysis. The Best7 is shown to have the smallest errors for the historical period, especially for storm central pressure, cyclogenesis, and deepening rates. The Best7 models encompass six of the seven highest-resolution CMIP models.

There is a relatively large decadal variability in the number of cyclones in the CFSR from 1979–2004 over eastern North America and the western Atlantic, with a 5%–10% increase in the mid-to-late 1980s and late 1990s. There is a slight downward trend in the number of cyclones since the early 1990s. The individual CMIP models also simulate large interdecadal variability peaking at various times, thus contributing to the 20%–30% difference between models.

There is a decrease in cyclone track density over the western Atlantic storm track from 5% to 10% in the early twenty-first century (2009–38) to 10%–30% by the late-twenty-first century (2069–98) in the Best7. This is in agreement with other studies focusing on this same region (Teng et al. 2008; Long et al. 2009). There is also a 5%–20% decrease in track density around the Great Lakes and to the east of southern Greenland by the late-twenty-first century. Meanwhile, there is a 5%–20% increase in track density along the eastern North American coast, which differs from recent studies using 1–2 models (Long et al. 2009; Teng et al. 2008). These future changes are 20%–30% weaker in the mean for the other (more coarse resolution) models for most locations. Previous studies have shown a decrease in the cyclone numbers for Northern Hemisphere winter (e.g., Lambert 1995; Geng and Sugi 2003; Bengtsson et al. 2006; Lambert and Fyfe 2006; Pinto et al. 2007; Catto et al. 2011), but our results also emphasize the regional nature of the future changes around eastern North America.

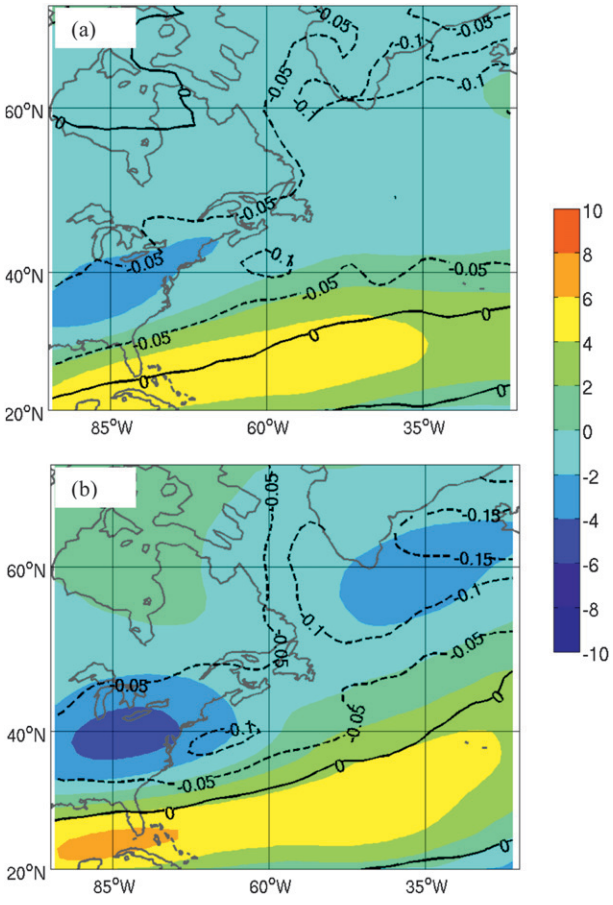

FIG. 18. Difference in the Eady growth rate (contoured every 0.05 day^{-1}) and 250-hPa wind speed (shaded every 2 m s^{-1}) between the 2069 and 2098 minus the historical (1979–2004) period for the (a) CNRM-CM5 and (b) MIROC5.

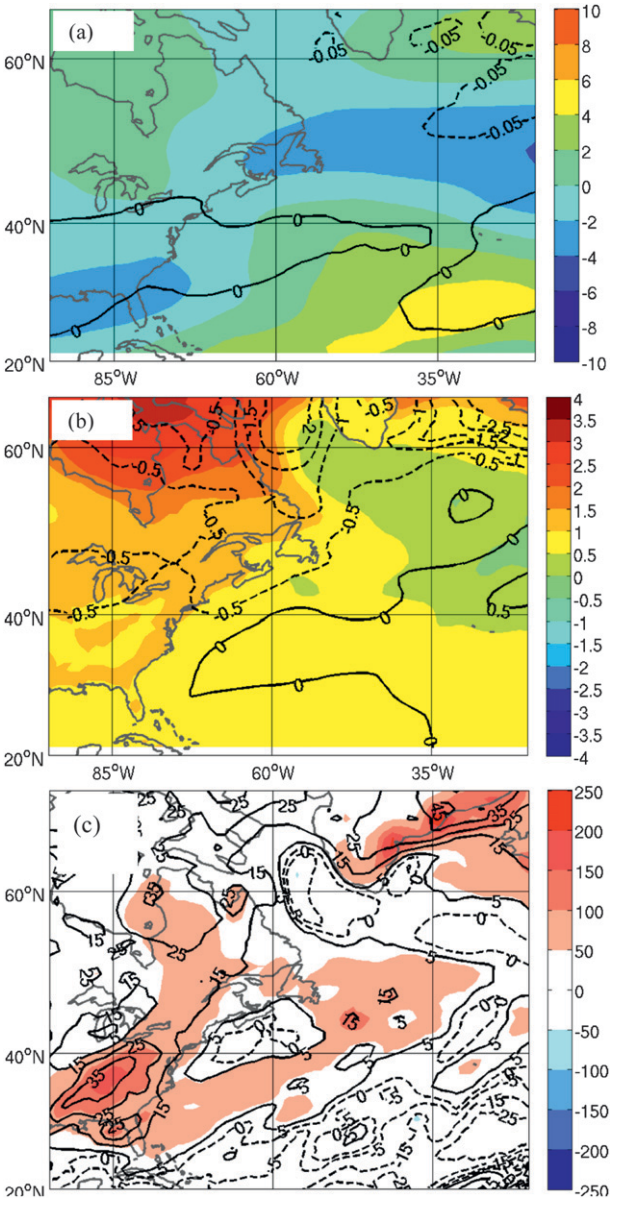

FIG. 19. (a) As in Fig. 18, but for the CCSM4 showing the difference between the mid-twenty-first century (2039–68). (b) Difference in average surface temperature (°C) and temperature gradient [°C (1000 km)$^{-1}$], and (c) precipitation (shaded in mm per cold season) between mid-twenty-first century (2039–2068) and the past (1979–2004). The percentage precipitation difference is contoured every 10%, with negative dashed.

Previous studies have suggested that the central pressure of the more extreme extratropical cyclones may intensify (Mizuta et al. 2011; Jiang and Perrie 2007; Long et al. 2009). In our study, by the late-twenty-first century the number of relatively deep (<980 hPa) storms over the western Atlantic in the Best7 mean decreases by ~10%, whereas there is a 12% decrease for relatively weak (1000–1010 hPa) storms. In contrast for over inland locations along the U.S. East Coast and eastern Canada, there is a 10%–40% increase in the number of relatively deep (<980 hPa) cyclones, which peaks in the mid-twenty-first century. There is little change in the number of strong storms over the Atlantic along the East Coast, while there is a 5%–15% decrease in the number of relatively weak storms. There are also 20%–40% more storms deepening >5 hPa in 6 h along the eastern United States The maximum 850-hPa winds within 10° around the cyclone center were analyzed for two models (MPI-ESM-LR and MRI-CGCM3) for the U.S. East Coast region, and there was a 15%–45% increase in periods >34 m s^{-1}.

Results based on CCSM4 and MRI-CGCM3 suggest that the increase along the East Coast may be related to increased latent heating during the next century, since there was little change in Eady growth rates, jet strength, and temperature gradient, but there was 5%–30% more

precipitation for this part of the storm track. Overall, these results suggest that although cyclones will be weaker and less frequent over much of the western Atlantic storm track, cyclones may become more intense and deepen more rapidly just inland of the U.S. East Coast, especially during the mid-twenty-first century.

These results emphasize the regional differences in cyclone changes around eastern North America and the importance of model resolution in simulating these changes. Future work will involve dynamically downscaling select CMIP5 models using mesoscale models to determine the robustness of these CMIP5 results, as well as determine mechanisms for the increase in stronger storms along the U.S. East Coast.

Acknowledgments. We appreciate the constructive comments by the three anonymous reviewers. We thank Dr. Kevin Hodges for use of his TRACK software. The authors acknowledge the support of NOAA Climate Program Office Modeling, Analysis, Predictions and Projections (MAPP) Program as part of the CMIP5 Task Force under Grant NA11OAR4310104, the DOE Office of Science through its Office of Biological and Environmental Sciences, and the National Sea Grant College Program of NOAA (NYSG R/RCP-17). We acknowledge the World Climate Research Programme's Working Group on Coupled Modeling, which is responsible for CMIP, and we thank the climate modeling groups (listed in Table 1 of this paper) for producing and making available their model output. For CMIP, the U.S. Department of Energy's Program for Climate Model Diagnosis and Intercomparison provides coordinating support and led development of software infrastructure in partnership with the Global Organization for Earth System Science Portals.

REFERENCES

Anderson, D., K. I. Hodges, and B. J. Hoskins, 2003: Sensitivity of feature-based analysis methods of storm tracks to the form of background field removal. *Mon. Wea. Rev.,* **131,** 565–573.

Bengtsson, L., K. I. Hodges, and E. Roeckner, 2006: Storm tracks and climate change. *J. Climate,* **19,** 3518–3543.

Carnell, R. E., and C. A. Senior, 1998: Changes in mid-latitude variability due to increasing greenhouse gases and sulfate aerosols. *Climate Dyn.,* **14,** 369–383.

Catto, J. L., L. C. Shaffrey, and K. I. Hodges, 2011: Northern Hemisphere extratropical cyclones in a warming climate in the HiGEM high-resolution climate model. *J. Climate,* **24,** 5336–5352.

Chang, K. M., Y. Guo, Z. Xia, and M. Zheng, 2013: Storm-track activity in IPCC AR4/CMIP5 model simulations. *J. Climate,* **26,** 246–260.

Colle, B. A., 2003: Numerical simulations of the extratropical transition of Floyd (1999): Structural evolution and responsible mechanisms for the heavy rainfall over the Northeast United States. *Mon. Wea. Rev.,* **131,** 2905–2926.

——, F. Buonaiuto, M. J. Bowman, R. E. Wilson, R. Flood, R. Hunter, A. Mintz, and D. Hill, 2008: New York City's vulnerability to coastal flooding. *Bull. Amer. Meteor. Soc.,* **89,** 829–841.

——, K. Rojowsky, and F. Buonaiuto, 2010: New York City storm surges: Climatology and analysis of the wind and cyclone evolution. *J. Appl. Meteor. Climatol.,* **49,** 85–100.

Dee, D. P., and Coauthors, 2011: The ERA-Interim reanalysis: Configuration and performance of the data assimilation system. *Quart. J. Roy. Meteor. Soc.,* **137,** 553–597.

Donner, L. J., and Coauthors, 2011: The dynamical core, physical parameterizations, and basic simulation characteristics of the atmospheric component AM3 of the GFDL global coupled model CM3. *J. Climate,* **24,** 3484–3519.

Dufresne, J.-L., and Coauthors, 2013: Climate change projections using the IPSL-CM5 Earth system model: From CMIP3 to CMIP5. *Climate Dyn.,* **40,** 2123–2165.

Geng, Q., and M. Sugi, 2003: Possible change of extratropical cyclone activity due to enhanced greenhouse gases and sulfate aerosols—Study with a high-resolution AGCM. *J. Climate,* **16,** 2262–2274.

Gent, P. R., and Coauthors, 2011: The Community Climate System Model version 4. *J. Climate,* **24,** 4973–4991.

Harvey, B. J., L. C. Shaffrey, T. J. Woollings, G. Zappa, and K. I. Hodges, 2012: How large are projected 21st century storm track changes? *Geophys. Res. Lett.,* **39,** L18707, doi:10.1029/2012GL052873.

Hazeleger, W., and Coauthors, 2010: EC-Earth: A seamless Earth system prediction approach in action. *Bull. Amer. Meteor. Soc.,* **91,** 1357–1363.

Held, I. M., and E. O'Brien, 1992: Quasigeostrophic turbulence in a three-layer model: Effects of vertical structure in the mean shear. *J. Atmos. Sci.,* **49,** 1861–1870.

Hirsch, M. E., A. T. DeGaetano, and S. J. Colucci, 2001: An East Coast winter storm climatology. *J. Climate,* **14,** 882–899.

Hodges, K. I., 1994: A general method for tracking analysis and its application to meteorological data. *Mon. Wea. Rev.,* **122,** 2573–2586.

——, 1995: Feature tracking on the unit sphere. *Mon. Wea. Rev.,* **123,** 3458–3465.

——, R. W. Lee, and L. Bengtsson, 2011: A comparison of extratropical cyclones in recent reanalyses ERA-Interim, NASA MERRA, NCEP CFSR, and JRA-25. *J. Climate,* **24,** 4888–4906.

Hoskins, B. J., and P. J. Valdes, 1990: On the existence of storm-tracks. *J. Atmos. Sci.,* **47,** 1854–1864.

——, and K. I. Hodges, 2002: New perspectives on the Northern Hemisphere winter storm tracks. *J. Atmos. Sci.,* **59,** 1041–1061.

Jiang, J., and W. Perrie, 2007: The impacts of climate change on autumn North Atlantic midlatitude cyclones. *J. Climate,* **20,** 1174–1187.

Jones, C. D., and Coauthors, 2011: The HadGEM2-ES implementation of CMIP5 centennial simulations. *Geosci. Model Dev.,* **4,** 543–570, doi:10.5194/gmd-4-543-2011.

Joyce, T. M., Y.-O. Kwon, and L. Yu, 2009: On the relationship between synoptic wintertime atmospheric variability and path shifts in the Gulf Stream and the Kuroshio Extension. *J. Climate,* **22,** 3177–3192.

Jung, T., S. K. Gulev, I. Rudeva, and V. Soloviov, 2006: Sensitivity of extratropical cyclone characteristics to horizontal resolution in the ECMWF model. *Quart. J. Roy. Meteor. Soc.,* **132,** 1839–1857, doi:10.1256/qj.05.212.

Jungclaus, J. H., and Coauthors, 2006: Ocean circulation and tropical variability in the coupled model ECHAM5/MPIOM. *J. Climate,* **19,** 3952–3972.

Knippertz, P., U. Ulbrich, and P. Speth, 2000: Changing cyclones and surface wind speeds over the North Atlantic and Europe in a transient GHG experiment. *Climate Res.,* **15,** 109–122.

Lambert, S. J., 1995: The effect of enhanced greenhouse warming on winter cyclone frequencies and strengths. *J. Climate,* **8,** 1447–1452.

——, and J. C. Fyfe, 2006: Changes in winter cyclone frequencies and strengths simulated in enhanced greenhouse warming experiments: Results from the models participating in the IPCC diagnostic exercise. *Climate Dyn.,* **26,** 713–728.

Leibensperger, E. M., L. J. Mickley, and D. J. Jacob, 2008: Sensitivity of US air quality to mid-latitude cyclone frequency and implications of 1980–2006 climate change. *Atmos. Chem. Phys.,* **8,** 7075–7086.

Long, Z., W. Perrir, J. Gyakum, R. Laprisee, and D. Caya, 2009: Scenario changes in the climatology of winter midlatitude cyclone activity over eastern North America and the northwest Atlantic. *J. Geophys. Res.,* **114,** D12111, doi:10.1029/2008JD010869.

Lunkeit, F., K. Fraedrich, and S. E. Bauer, 1998: Storm tracks in a warmer climate: Sensitivity studies with a simplified global circulation model. *Climate Dyn.,* **14,** 813–826.

Meehl, G. A., C. Covey, T. Delworth, M. Latif, B. McAveny, J. F. B. Mitchell, R. J. Stouffer, and K. E. Taylor, 2007: The WCRP CMIP3 multimodel dataset: A new era in climate change research. *Bull. Amer. Meteor. Soc.,* **88,** 1383–1394.

Michou, M., and Coauthors, 2011: A new version of the CNRM chemistry-climate model, CNRM-CCM: Description and improvements from the CCMVal-2 simulations. *Geosci. Model Dev. Discuss.,* **4,** 1129–1183.

Mickley, L. J., D. J. Jacob, B. D. Field, and D. Rind, 2004: Effects of future climate change on regional air pollution episodes in the United States. *Geophys. Res. Lett.,* **31,** L24103, doi:10.1029/2004GL021216.

Mizuta, R., M. Matsueda, H. Endo, and S. Yukimoto, 2011: Future change in extratropical cyclones associated with change in the upper troposphere. *J. Climate,* **24,** 6456–6470.

Novak, D., B. A. Colle, and S. Yuter, 2008: High resolution observations and model simulations of an intense mesoscale snowband. *Mon. Wea. Rev.,* **136,** 1433–1456.

Paciorek, C., J. Risbey, V. Ventura, and R. Rosen, 2002: Multiple indices of Northern Hemisphere cyclone activity, winters 1949–1999. *J. Climate,* **15,** 1573–1590.

Pinto, J. G., U. Ulbrich, G. C. Leckebusch, T. Spangehl, M. Reyers, and S. Zacharias, 2007: Changes in storm track and cyclone activity in three SRES ensemble experiments with the ECHAM5/MPI-OM1 GCM. *Climate Dyn.,* **29,** 195–210.

Saha, S., and Coauthors, 2010: The NCEP Climate Forecast System Reanalysis. *Bull. Amer. Meteor. Soc.,* **91,** 1015–1057.

Salari, V., and I. K. Sethi, 1990: Feature point correspondence in the presence of occlusion. *IEEE Trans. Pattern Anal. Mach. Intell.,* **12,** 87–91.

Sheffield, J., and Coauthors, 2013: North American climate in CMIP5 experiments. Part I: Evaluation of historical simulations of continental and regional climatology. *J. Climate,* in press.

Simmonds, I., and E.-P. Lim, 2009: Biases in the calculation of Southern Hemisphere mean baroclinic eddy growth rate. *Geophys. Res. Lett.,* **36,** L01707, doi:10.1029/2008GL036320.

Taylor, K. E., R. J. Stouffer, and G. A. Meehl, 2012: An overview of CMIP5 and the experiment design. *Bull. Amer. Meteor. Soc.,* **93,** 485–498.

Teng, H., W. M. Washington, and G. A. Meehl, 2008: Interannual variations and future change of wintertime extratropical cyclone activity over North America in CCSM3. *Climate Dyn.,* **30,** 673–686, doi:10.1007/s00382-007-0314-1.

Ulbrich, U., J. G. Pinto, H. Kupfer, G. C. Leckebusch, T. Spangehl, and M. Reyers, 2008: Changing Northern Hemisphere storm tracks in an ensemble of IPCC climate change simulations. *J. Climate,* **21,** 1669–1679.

Volodin, E. M., N. A. Dianskii, and A. V. Gusev, 2010: Simulating present day climate with the INMCM4.0 coupled model of the atmospheric and oceanic general circulations. *Atmos. Oceanic Phys.,* **46,** 414–431.

Watanabe, S., and Coauthors, 2011: MIROC-ESM: Model description and basic results of CMIP5-20c3m experiments. *Geosci. Model Dev.,* **4,** 845–872.

Woollings, T., B. Hoskins, M. Blackburn, D. Hassell, and K. Hodges, 2010: Storm track sensitivity to sea surface temperatures resolution in a regional atmosphere model. *Climate Dyn.,* **35,** 343–353.

——, J. M. Gregory, J. G. Pinto, M. Reyers, and D. J. Brayshaw, 2012: Response of the North Atlantic storm track to climate change shaped by ocean-atmosphere coupling. *Nat. Geosci.,* **5,** 313–317.

Wu, T., and Coauthors, 2010: The Beijing Climate Center for atmospheric general circulation model: Description and its performance for the present-day climate. *Climate Dyn.,* **34,** 123–147, doi:10.1007/s00382-008-0487-2.

Yin, J., 2005: A consistent poleward shift of the storm tracks in simulations of the 21st century climate. *Geophys. Res. Lett.,* **32,** L18701, doi:10.1029/2005GL023684.

Yukimoto, S., and Coauthors, 2012: A new global climate model of the Meteorological Research Institute: MRI-CGCM3—Model description and basic performance. *J. Meteor. Soc. Japan,* **90A,** 23–64.

Zanchettin, D., A. Rubino, D. Matei, O. Bothe, and J. H. Jungclaus, 2012: Multidecadal-to-centennial SST variability in the MPI-ESM simulation ensemble for the last millennium. *Climate Dyn.,* **39,** 419–444, doi:10.1007/s00382-012-1361-9.

Zhang, K., B. C. Douglas, and S. P. Leatherman, 2000: Twentieth-century storm activity along the U.S. East Coast. *J. Climate,* **13,** 1748–1761.

Zhang, Y., and W.-C. Wang, 1997: Model-simulated northern winter cyclone and anticyclone activity under a greenhouse warming scenario. *J. Climate,* **10,** 1616–1634.

Zhang, Z. S., and Coauthors, 2012: Pre-industrial and mid-Pliocene simulations with NorESM-L. *Geosci. Model Dev.,* **5,** 523–533, doi:10.5194/gmd-5-523-2012.